THE UNIVERSITY OF CHICAGO

VARIATIONAL TWO-ELECTRON REDUCED DENSITY MATRIX THEORY OF PERIODIC SYSTEMS

A DISSERTATION SUBMITTED TO
THE FACULTY OF THE DIVISION OF THE PHYSICAL SCIENCES
IN CANDIDACY FOR THE DEGREE OF
DOCTOR OF PHILOSOPHY

DEPARTMENT OF CHEMISTRY

BY
SIMON EWING

CHICAGO, ILLINOIS
JUNE 2022

To Hayley, Elliott, Teri, Bob, and Barbara

TABLE OF CONTENTS

LIST OF FIGURES

LIST OF TABLES

ACKNOWLEDGMENTS

First of all, I'd like to thank my advisor, David Mazziotti, for his support throughout my graduate career. His kindness and perseverance when I faced challenges helped instill in me the determination to tackle problems and follow them through to their conclusion. I'd also like to thank the other members of the Mazziotti group who, through casual conversations or intellectually rigorous discussions of our work, helped keep me focused and grounded throughout my time at the University of Chicago, particularly: Nik, Scott, Danny, Guan, LeeAnn, Jordan, Olivia, Manas, Ali, Kade, Anthony, and Sam.

I can't thank my family enough for having the patience to endure my rants about my work even though they often didn't know what I was talking about. My fiance Hayley, in particular, patiently listened to me talk about my struggles, challenges, and triumphs on a daily basis, and I can't thank her enough. My dad, Bob, often challenged how I communicate my work by suggesting metaphors and parallels that I wouldn't have thought of otherwise. My brother, Elliott, helped me learn how to program and has been there from the beginning of my academic career (personal or professional) with help when I needed it. Finally, my mom, Teri, has frequently lent her words of wisdom when I faced tough decisions or situations, and reminded me to enjoy myself during my time in grad school.

Finally, I'd like to thank my undergraduate advisor, Dr. Jim Prell, for introducing me to the world of research and fostering in me a love of the pursuit of knowledge. Without his generous offer to support my undergraduate work, I'm certain that I wouldn't be in the position that I'm in today.

ABSTRACT

The recovery of static correlation through electronic structure calculations has led to many novel insights and more accurate prediction of chemical properties for many molecular systems which exhibit a high degree of degeneracy. However, such calculations are often prohibitively expensive for nontrivial systems when using wavefunction-based methods. The use of Reduced Density Matrix (RDM) theories can lessen the computational cost, leading to the possibility of computing electron structures for larger systems that include static correlation. Here, the Variational 2-electron Reduced Density Matrix (v2RDM) theory is applied to periodic systems both in the gamma-point representation and utilizing Brillouin Zone sampling, to analyze how static correlation is affected by periodic boundary conditions and to determine whether static correlation is affected by the momentum of the underlying periodic basis functions. Additionally, the amount of static correlation present in a system is quantified using an adapted form of the Von Neumann Entropy which incorporates 3-body correlation while remaining size-extensive. I show that static correlation is an important factor in the electronic structure of periodic materials, and that in some cases the static correlation in periodic materials is more significant than in their molecular counterparts.

CHAPTER 1

INTRODUCTION

1.1 Hartree-Fock Approximations and Correlation

Through the time-independent, non-relativistic Schrödinger equation, the electronic state of a quantum system can be determined by solving

$$\hat{H}|\Psi_n\rangle = E_n|\Psi_n\rangle \tag{1.1}$$

where $\hat{H}$ is the Hamiltonian, E_n are the energies in the system's spectrum, and $|\Psi_n\rangle$ are the state vectors for each energy state. Due to electron-electron terms in the Hamiltonian, the Schrödinger equation can only be solved exactly for one-electron systems, and so approximation methods are used to solve the Schrödinger equation for many-electron systems.

The simplest and most commonly-used approximation method is the Hartree-Fock method,[1–3] in which the state vector is approximated as a single slater determinant,[4] defined as

$$|\Psi_{HF}\rangle = \bigwedge_i^N \zeta_i(i) = \zeta_1(1) \wedge \zeta_2(2) \wedge \cdots \wedge \zeta_N(N) \tag{1.2}$$

where (i) indicates the spin and spatial coordinates for electron i and the $\wedge$ operator represents the antisymmetric tensor product that combines an N-electron state with a 1-electron to form an $N+1$-electron state. The basis functions ζ_i represent the molecular orbitals, and they are chosen as orthonormal linear combinations of atomic orbitals such that the ground state energy of the N-electron state is minimized. The Hartree-Fock ansatz maintains the antisymmetry of the wavefunction while treating electron-electron interactions as a single electron in the mean field of the remaining $N-1$ electrons. The Hartree-Fock energy is minimized by solving the generalized eigenvalue problem in the Roothaan-Hall equations:[5,6]

$$FC = SCE \tag{1.3}$$

where $F = {}^1H + 2J - K$ is the Fock matrix, ${}^1H$ is the core (one-electron) integral matrix, J and K are the coulomb and exchange integrals, respectively, S is the atomic orbital overlap matrix, E is the diagonal matrix of molecular orbital energies, and C is the matrix of column vectors of molecular orbital coefficients. Because the J and K matrices depend on the 1-electron reduced density matrix (1-RDM), defined in restricted Hartree-Fock theory (where α and β electrons are restricted to have the same MO coefficients) as $2CC^T$, these equations must be solved self-consistently. That is, an initial guess 1-RDM is constructed which is used to compute an approximate J and K. The Roothaan-Hall equations are then solved to get a more accurate form of the MO coefficient matrix C, which can then be used to construct a more accurate 1-RDM. This process is repeated until the total energy of the system converges, and the 1-RDM ceases to change between iterations.

Due to the construction of the 1-RDM in Hartree-Fock theory, it is diagonal when represented in the MO basis. Furthermore, the diagonal elements are 1 (if the MO is occupied) or 0 (if the MO is unoccupied). This demonstrates that the eigenvalues of the 1-RDM in the MO basis are analogous to the number of electrons in molecular orbital, which we'll explore more in the next section.

1.2 Static Correlation from Electronic Structure Methods

The goal of post Hartree-Fock methods is to recover all or part of the electron correlation lost in Hartree-Fock through the mean field approximation. This correlation is usually categorized as dynamic or static correlation.[7–10] Dynamic correlation is defined as correlation due to the instantaneous position of pairs of electrons as they repel each other, whereas static correlation is due to near-degeneracies which make the single slater determinant approximation

invalid. Methods which focus on the form of the Hamiltonian such as Coupled Cluster,[11–13] Density Functional Theory,[14–16] perturbation theory,[17–19] and many others capture a significant portion of the dynamic correlation, whereas methods that focus on the form of the wavefunction such as FCI,[20,21] active space methods,[22,23] and multireference methods capture a significant portion of the static correlation. Despite the categorization, both types of correlation can be detected through the eigenvalues of the 1-RDM and higher-order reduced density matrices.

As mentioned in the previous section, the Hartree-Fock 1-RDM has eigenvalues of 1 or 0, indicating whether the MO is occupied or virtual. However, in general 1-RDMs can have eigenvalues anywhere in the range between 0 and 1, implying that MOs can be fractionally occupied in post-Hartree-Fock methods. As such, this fractional occupation is commonly used as a metric for how correlated a system is.[24,25] Dynamic correlation is usually represented by many occupations near 0 or 1 and static correlation is represented by a few occupations near 1/2. Chemically, this roughly corresponds to unpaired electrons in systems like radicals and high-spin systems.

Although interpretation of eigenvalues of higher order RDMs is more complicated than the 1-RDM, similar fractional occupation is observable in higher order correlated RDMs and can be interpreted in terms of static and dynamic correlation. In the extreme limit of the full N-electron density matrix, fractional occupations indicate that the system is in a mixed state, meaning that the electrons in the system are entangled with their surroundings. Although I'm going to focus on pure systems in this context, the comparison of eigenvalues of RDMs and the full density matrix can be helpful in understanding their interpretation. For example, the 2-RDM describes a physical 2-electron state coupled with its environment, which is the remaining $N-2$ mean field electrons. This comparison between mixed states and fractional occupations will be discussed further in Chapter 2 in reference to purity and various forms of entropy based on RDMs.

References

(1) Hartree, D. R. The Wave Mechanics of an Atom with a Non-Coulomb Central Field. Part II. Some Results and Discussion. *Mathematical Proceedings of the Cambridge Philosophical Society* **1928**, *24*, 111–132.

(2) Fock, V. Näherungsmethode zur Lösung des quantenmechanischen Mehrkörperproblems. *Zeitschrift für Physik 1930 61:1* **1930**, *61*, 126–148.

(3) Hartree, D. R.; Hartree, W. Self-consistent field, with exchange, for beryllium. *Proceedings of the Royal Society of London. Series A - Mathematical and Physical Sciences* **1935**, *150*, 9–33.

(4) Slater, J. C. Molecular Energy Levels and Valence Bonds. *Physical Review* **1931**, *38*, 1109.

(5) Roothaan, C. C. New Developments in Molecular Orbital Theory. *Reviews of Modern Physics* **1951**, *23*, 69.

(6) Hall, G. G. The molecular orbital theory of chemical valency VIII. A method of calculating ionization potentials. *Proceedings of the Royal Society of London. Series A. Mathematical and Physical Sciences* **1951**, *205*, 541–552.

(7) Hollett, J. W.; Gill, P. M. The two faces of static correlation. *The Journal of Chemical Physics* **2011**, *134*, 114111.

(8) Bulik, I. W.; Henderson, T. M.; Scuseria, G. E. Can Single-Reference Coupled Cluster Theory Describe Static Correlation? *Journal of Chemical Theory and Computation* **2015**, *11*, 3171–3179.

(9) Piris, M. Global Method for Electron Correlation. *Physical Review Letters* **2017**, *119*, 063002.

(10) Cremer, D. Density functional theory: coverage of dynamic and non-dynamic electron correlation effects. *http://dx.doi.org/10.1080/00268970110083564* **2009**, *99*, 1899–1940.

(11) Bartlett, R. J.; Musiał, M. Coupled-cluster theory in quantum chemistry. *Reviews of Modern Physics* **2007**, *79*, 291–352.

(12) *Reviews in computational chemistry*; Lipkowitz, K. B., Boyd, D. B., Eds.; Wiley Blackwell: 2000; Vol. 14, pp 33–136.

(13) Jeziorski, B.; Monkhorst, H. J. Coupled-cluster method for multideterminantal reference states. *Physical Review A* **1981**, *24*, 1668.

(14) Parr, R. G. Density Functional Theory of Atoms and Molecules. *Horizons of Quantum Chemistry* **1980**, 5–15.

(15) Hohenberg, P.; Kohn, W. Inhomogeneous electron gas. *Physical Review* **1964**, *136*, B864.

(16) Malet, F.; Gori-Giorgi, P. Strong correlation in Kohn-Sham density functional theory. *Physical Review Letters* **2012**, *109*, 246402.

(17) Møller, C.; Plesset, M. S. Note on an approximation treatment for many-electron systems. *Physical Review* **1934**, *46*, 618–622.

(18) Pople, J. A.; Krishnan, R.; Schlegel, H. B.; Binkley, J. S. Derivative studies in hartree-fock and møller-plesset theories. *International Journal of Quantum Chemistry* **1979**, *16*, 225–241.

(19) Tsuchimochi, T.; Scuseria, G. E. Strong correlations via constrained-pairing mean-field theory. *Journal of Chemical Physics* **2009**, *131*, 121102.

(20) Murray, C. W.; Racine, S. C.; Davidson, E. R. Improved algorithms for the lowest few eigenvalues and associated eigenvectors of large matrices. *Journal of Computational Physics* **1992**, *103*, 382–389.

(21) Eriksen, J. J.; Gauss, J. Incremental treatments of the full configuration interaction problem. *Wiley Interdisciplinary Reviews: Computational Molecular Science* **2021**, *11*, e1525.

(22) Roos, B. O.; Taylor, P. R.; Sigbahn, P. E. A complete active space SCF method (CASSCF) using a density matrix formulated super-CI approach. *Chemical Physics* **1980**, *48*, 157–173.

(23) Veryazov, V.; Malmqvist, P. Å.; Roos, B. O. How to select active space for multiconfigurational quantum chemistry? *International Journal of Quantum Chemistry* **2011**, *111*, 3329–3338.

(24) Helbig, N.; Tokatly, I. V.; Rubio, A. Physical meaning of the natural orbitals: Analysis of exactly solvable models. *Physical Review A - Atomic, Molecular, and Optical Physics* **2010**, *81*, 022504.

(25) Schlimgen, A. W.; Heaps, C. W.; Mazziotti, D. A. Entangled Electrons Foil Synthesis of Elusive Low-Valent Vanadium Oxo Complex. *Journal of Physical Chemistry Letters* **2016**, *7*, 627–631.

CHAPTER 2

QUANTIFYING CORRELATION USING QUANTUM ENTROPY

2.1 Von Neumann Entropy

As mentioned in the previous chapter, correlation can be identified as fractional occupation in RDMs. However, it can be constructive to reduce the occupations to a single value that represents the degree of correlation present in the system. There are many ways to contract the eigenvalues to a single real number, including the purity, linear entropy,[1–3] and Von Neumann entropy[4] (VNE), as well as a few of their generalizations such as the Renyi entropy,[5] or the Tsallis entropy.[6] Each of these metrics satisfies several important criteria for quantum entropies, but only the Von Neumann Entropy is concave, non-negative, and strongly sub-additive. These qualities are useful in drawing comparisons to the classical Boltzmann and Shannon entropies,[7] and despite the VNE's close connection to the Shannon entropy, these qualities were not proven to hold until the 1970's.[8] The VNE is defined as:

$$S_N = -\mathrm{Tr}({}^N D \ln {}^N D) \tag{2.1}$$

where ${}^N D$ is the full N-electron density matrix. The matrix logarithm is defined via the taylor series expansion of the natural logarithm function, similar to matrix exponentials. Because this taylor series depends only on powers of the density matrix, the trace in the Equation 2.1 can be replaced by a sum over the eigenvalues of the density matrix:

$$S_N = -\sum_i \xi_i \ln \xi_i \tag{2.2}$$

where ξ_i are eigenvalues of the density matrix. The minimal VNE is 0 (it is nonnegative), which occurs when the state is pure. Because pure states are idempotent, each of

their eigenvalues are 0 or 1, and therefore each term in the sum is exactly zero. Although $\ln(0)$ is undefined, the limit of $x\ln(x)$ as x approaches 0 is zero. At the other extreme, a maximally-mixed state approaches an entropy of $\ln(r)$ where r is the number of N-electron basis functions.

Because the VNE is simply the quantum analogue of the classical Shannon Entropy, it has all of the same properties like extensivity, concavity, and monotonicity with respect to decoherence. As a result, I will be using the VNE as a way to discuss electronic correlation throughout the rest of this paper. However, the full density matrix is quite often impractical or impossible to store, given the exponential scaling in the number of N-electron basis functions and because only the 2-RDM is needed to recover an exact energy. Furthermore, the VNE is more closely related to the degree of mixing of the state than the electronic correlation within the system. Therefore, if we want an entropy that measures electron correlation, we need to use a reduced entropy that is based on the properties of RDMs.

2.2 Reduced Entropies

If we use the 1-RDM instead of the full density matrix we get S_1, the 1-electron VNE. It can be shown that this form of entropy also satisfies the requirements in the previous section for comparison to the classical Shannon entropy, and therefore it has been used frequently to quantify correlation in electronic structure calculations. Because 1-RDMs can be recovered from all electronic structure methods, the 1-electron VNE can be calculated using any method. Because of its wide-ranging use, this is often simply called *the Von Neumann Entropy*, although that term is more accurately used to describe the quantity in Eq. 2.1.

However, the 2-electron VNE S_2 is not extensive like S_1 or ${S_N}^9$ (except in the case where $N = 2$), and so it cannot generally be directly used as a measure of entropy. If we want to use the 2-RDM occupations to quantify high-order correlation, we need to modify S_2 to

produce an entropy measure that is extensive. See Theorem 1 for a proof that the connected 2-electron VNE, defined as $S_C = S_2 - 2NS_1$, satisfies extensivity.

The 1-electron VNE can be interpreted as a way to quantify the degree of correlation between individual electrons and their surroundings, known as bipartite correlation. Similarly, the connected 2-electron VNE quantifies the degree of correlation between electron pairs and their surroundings, or tripartite correlation.[10,11] In essence, the construction of the connected 2-electron VNE simply removes correlation from electron pairs where the electrons exist in different subsystems, but still captures the bipartite and tripartite correlation within each subsystem. Therefore, both the 1-electron VNE and connected 2-electron VNE can be used together to classify the type of correlation and quantify the amount of correlation present in a system.

In physical systems, higher order correlation can exist than tripartite correlation. However, without the use of higher order RDMs, recovery of those types of correlation remains a challenge. This highlights one limitation of using the 2-RDM as the basic variable in calculations, since higher-order RDMs can only be approximately constructed through various techniques.[12,13] By contrast, a full treatment of the wavefunction as in FCI can theoretically recover RDMs of any order, given enough computational time and memory. As such, one potential route forward with this theory would be to define higher-order equivalents of the 2-electron connected entropy, which will be closely related to the cumulant expansion of the p-RDMs, to assemble a hierarchy of connected entropies for use in wavefunction-based methods (or to be approximated in 2-RDM methods) which could quantify higher-order correlation in the system.

Theorem 1. *The connected 2-electron Von Neumann Entropy, $S_C = S_2 - 2NS_1$, is extensive.*

Proof. First, note that the 2-RDM can be expanded using the cumulant as ${}^2D_{AB} = {}^1D_{AB} \wedge {}^1D_{AB} + {}^2\Delta_{AB} = {}^2W_{AB} + {}^2\Delta_{AB}$ where I've defined ${}^2W = {}^1D \wedge {}^1D$ for notational clarity. To

show that S_C is extensive, we need to that if $\Psi = \Psi_A \wedge \Psi_B$ then $S_C(\Psi) = S_C(\Psi_A) + S_C(\Psi_B)$. For this form of wavefunction, both the 1-RDM and the 2-RDM cumulant are additively separable so that

$$^1D_{AB} = {}^1D_A + {}^1D_B \tag{2.3}$$

$$^2\Delta_{AB} = {}^2\Delta_A + {}^2\Delta_B \tag{2.4}$$

Therefore, only terms related to $^2W_{AB}$ need to be considered because the other terms will contribute equally to $S_C(\Psi_A)$ and $S_C(\Psi_B)$. Using Lemma 1.1, we need to include the $2NS_1$ term, since $2NS_1 = S_2\left(^2W_{AB}\right)$. Therefore, we can expand the remaining terms as

$$-\operatorname{Tr}\left(^2W_{AB} \ln {}^2D_{AB}\right) + \operatorname{Tr}\left(^2W_{AB} \ln {}^2W_{AB}\right) \tag{2.5}$$

$$= -\operatorname{Tr}\left(^2W_{AB}\left(\ln {}^2D_{AB} - \ln {}^2W_{AB}\right)\right) \tag{2.6}$$

However, we can use the additivity of ^1D to write $^2W_{AB} = {}^2W_A + {}^2W_B + 2{}^1D_A \wedge {}^1D_B$. The first two terms contribute equally to each subsystem's entropy, so only the third term which describes the connection between subsystems A and B needs to be included. Using this fact, we can further simplify the remaining terms

$$-\operatorname{Tr}\left(^2W_{AB}\left(\ln {}^2D_{AB} - \ln {}^2W_{AB}\right)\right) \tag{2.7}$$

$$= -\operatorname{Tr}\left({}^1D_A \wedge {}^1D_B\left(\ln {}^2D_{AB} - \ln(^2W_{AB}\right)\right) \tag{2.8}$$

Because $^1D_A \wedge {}^1D_B$ is nonzero only for indices that mix subsystems and $^2\Delta_{AB}$ is nonzero only for indices within a single subsystem, the $\ln {}^2D_{AB}$ part of the first term can be simplified to $\ln {}^2W_{AB}$. Clearly then, this full expression is always equal to zero. Therefore, the only

nonzero terms contribute equally to the subsystem entropies such that $S_C(\Psi) = S_C(\Psi_A) + S_C(\Psi_B)$, and so S_C is extensive. □

Lemma 1.1. *Defining* ${}^2W = {}^1D \wedge {}^1D$*, we get that* $S_2\left({}^2W\right) = 2NS_1$.

Proof. Since the wedge operator is a form of tensor product, the eigenvalues of ${}^2W$ are equal to $\lambda_i\lambda_j$ where λ_i are the eigenvalues of ${}^1D$. Therefore, since $\mathrm{Tr}({}^1D) = \sum_i \lambda_i = N$,

$$S_2 = -\sum_{ij} \lambda_i\lambda_j \ln \lambda_i\lambda_j = -\sum_{ij} \lambda_i\lambda_j \ln \lambda_i - \sum_{ij} \lambda_i\lambda_j \ln \lambda_j \tag{2.9}$$

$$S_2 = N\left(-\sum_i \lambda_i \ln \lambda_i - \sum_j \lambda_j \ln \lambda_j\right) = 2NS_1 \tag{2.10}$$

□

References

(1) Jaeger, G., *Quantum Information: An Overview*; Springer Science: 2007, pp 5–10.

(2) Zanardi, P.; Zalka, C.; Faoro, L. Entangling power of quantum evolutions. *Physical Review A* **2000**, *62*, 030301.

(3) Peters, N. A.; Wei, T. C.; Kwiat, P. G. Mixed-state sensitivity of several quantum-information benchmarks. *Physical Review A* **2004**, *70*, 052309.

(4) Von Neumann, J., *Mathematische Grundlagen der Quantenmechanic*; Springer: 1932.

(5) Rényi, A. On Measures of Entropy and Information. *Mathematical Institute, Hungarian Academy of Sciences* **1961**, 547–561.

(6) Tsallis, C. Possible generalization of Boltzmann-Gibbs statistics. *Journal of Statistical Physics* **1988**, *52*, 479–487.

(7) Życzkowski, K. Renyi extrapolation of Shannon entropy. *Open Systems and Information Dynamics* **2003**, *10*, 297–310.

(8) Araki, H.; Lieb, E. H. Entropy inequalities. *Comm. Math. Phys.* **1970**, *18*, 160–170.

(9) Luzanov, A. V.; Prezhdo, O. High-order entropy measures and spin-free quantum entanglement for molecular problems. *Molecular Physics* **2007**, *105*, 2879–2891.

(10) Szalay, S. The classification of multipartite quantum correlation. *Journal of Physics A* **2018**, *51*, 485302.

(11) Guo, X.; Ma, C. T. Tripartite Entanglement and Quantum Correlation. *Journal of High Energy Physics* **2021**, *2021*, DOI: 10.48550/arxiv.2103.02983.

(12) Kutzelnigg, W.; Mukherjee, D. Cumulant expansion of the reduced density matrices. *The Journal of Chemical Physics* **1999**, *110*, 2800–2809.

(13) Deprince, A. E.; Mazziotti, D. A. Cumulant reconstruction of the three-electron reduced density matrix in the anti-Hermitian contracted Schrödinger equation. *The Journal of Chemical Physics* **2007**, *127*, 104104.

CHAPTER 3

PERIODIC BOUNDARY CONDITIONS AND THE BRILLOUIN ZONE

3.1 The Brillouin Zone and Wavefunction Methods

When calculating properties of extended systems like crystals, materials, and polymers, we often make the simplifying assumption that the atoms lie on a lattice, which imposes periodic boundary conditions on the system. Because the atoms lie on a lattice, the potential energy surface repeats every primitive unit cell, and according to Bloch's theorem[1] basis functions used to construct the wavefunction are constrained to the form

$$|\phi_j^{\mathbf{k}}(\mathbf{r})\rangle = e^{i\mathbf{k}\cdot\mathbf{r}}|u_j(\mathbf{r})\rangle \tag{3.1}$$

where $u_j(\mathbf{r})$ has the periodicity of the lattice. One way to summarize this result is that the wavefunction can change phase by a constant amount between primitive unit cells, and the amount that the phase can change is related to the crystal momentum vector $\mathbf{k}$. Since complex phase is periodic, the reciprocal space which the crystal momentum vector lies on is also periodic. As such, calculations for extended systems have a real-space lattice defined by the lattice of atomic coordinates as well as a reciprocal space lattice which is defined by the unique crystal momentum vectors. The cluster of points in reciprocal space that are closer to the origin than any other lattice point is called the Brillouin Zone, and it's the only region in momentum space that needs to be considered to exactly recover the state of a periodic system. However, the definition of the Brillouin Zone is not unique, due to the periodicity of reciprocal space. This definition is the most *compact* definition of the Brillouin Zone, but another common definition of the Brillouin Zone is the triclinic cell defined by the periodicity of the reciprocal lattice, which has a straightforward derivation from the real-space triclinic

cell.

Because the family of basis functions now depends on the crystal momentum vector, the treatment of periodic systems is only exact when the Brillouin Zone is densely sampled.[2–6] One common sampling technique uses a Monkhorst-Pack grid,[7] which uniformly divides the Brillouin Zone into parallelepipeds and each vertex in the tesselation of the Brillouin Zone is used as a sample point. Choice of Brillouin Zone sampling scheme is important to exploit additional symmetries like time-reversal symmetry and point-group symmetry, and can be used to equate the properties of individual k-points and reduce computational complexity without sacrificing accuracy.[8,9]

The benefits of using Brillouin Zone sampling are especially pronounced when used in the context of 1-electron methods. The 1-electron integrals (as well as the J and K matrices in Hartree-Fock theory) are block diagonal when sampling the Brillouin Zone, with one block per sampled k-point due to the conservation of momentum. Therefore, the use of Brillouin Zone sampling reduces 1-electron methods to individual subproblems for each k-point sampled. By contrast, the 2-electron basis functions are composed of pairs of 1-electron basis functions and so the block structure imposed by the conservation of momentum is more complicated; the 2-electron integrals have one block per total momentum, defined as $k_1 + k_2$ the sum of the momentum of each 1-electron basis function composing the 2-electron basis functions. Each block is composed of up to N_k^2 subblocks, where N_k is the number of k-points sampled. For this reason, the vast majority of electronic structure calculations on extended systems use either Hartree-Fock theory or Density Functional Theory.

3.2 Bases in Periodic systems

One benefit of sampling the Brillouin Zone using a Monkhorst-Pack grid of size $N_a \times N_b \times N_c$ is that all basis functions repeat within an integer number of real-space unit cells. That means that the total wavefunction must repeat on a supercell of size $N_a \times N_b \times N_c$, and we can

use a unitary transformation to convert between the k-point basis and a gamma-point basis on the supercell. Specifically, we can index the basis functions by their supercell translation vector and convert between the two with

$$|\phi_j^{\mathbf{T_i}}(\mathbf{r})\rangle = |\phi_j(\mathbf{r} - \mathbf{T_i})\rangle = \sum_m e^{-i\mathbf{k_m}\cdot\mathbf{T_i}} |\phi_j^{\mathbf{k_m}}(\mathbf{r})\rangle = \sum_m P^{im} |\phi_j^{\mathbf{k_m}}(\mathbf{r})\rangle \tag{3.2}$$

where $P_{im} = e^{-i\mathbf{k_i}\cdot\mathbf{T_i}}$ is the unitary (phase) transformation matrix. One benefit of performing this transformation is that if the system has time-reversal symmetry (which relates the $+\mathbf{k}$ and $-\mathbf{k}$ blocks of the electron integrals by complex conjugate), then the 1-electron and 2-electron integrals in the gamma-point basis will be real, so this transformation is one method of "realizing" the k-point system. Reasons for choosing a basis which realizes the electronic integrals are discussed in Chapter 4.

We have developed a 2nd method of realizing a k-point system, inspired by the direct realization of complex numbers. Specifically, the real part of a complex number is $\mathrm{Re}(z) = z + z^*$ and the imaginary part is $\mathrm{Im}(z) = -i(z - z^*)$. Similarly, we can define an adapted form of of k-point basis functions as:

$$|\chi^0\rangle = |\phi^0\rangle \tag{3.3}$$

$$|\chi_\alpha^{\mathbf{k}}\rangle = \frac{1}{\sqrt{2}} \left(|\phi^{\mathbf{k}}\rangle + |\phi^{-\mathbf{k}}\rangle \right) \tag{3.4}$$

$$|\chi_\beta^{\mathbf{k}}\rangle = -\frac{i}{\sqrt{2}} \left(|\phi^{\mathbf{k}}\rangle - |\phi^{-\mathbf{k}}\rangle \right) \tag{3.5}$$

Similarly to the gamma-point transformation, this k-adapted transformation realizes the system when it has time-reversal symmetry. However, this transformation only mixes the $\pm\mathbf{k}$ blocks, resulting in integrals with half of the block structure due to the conservation of momentum. By contrast, the gamma-point integrals don't retain any of the blocking structure due to the conservation of momentum. Therefore, computed matrices such as the

fock matrix, 1-RDM, 2-RDM, etc. have more blocking structure in the k-adapted basis than in the gamma-point basis while remaining real, which opens the door to computational and memory efficiency benefits when using this basis.

One final basis which can be used to realize the electron integrals is the direct realization basis, where each basis vector is replaced by two basis vectors: one representing the real part of the vector and one representing the imaginary part of the vector. This basis does not assume symmetry of the k-point integrals like the other two bases, and therefore will realize any periodic system due to the direct comparison between the real and imaginary components. This basis will be the subject of future work, especially in relation to v2RDM introduced in the next chapter.

References

(1) Bloch, F. Über die Quantenmechanik der Elektronen in Kristallgittern. *Zeitschrift für Physik 1929 52:7* **1929**, *52*, 555–600.

(2) Filippini, G.; Gramaccioli, C. M.; Simonetta, M.; Suffritti, G. B. Lattice-dynamical applications to crystallographic problems: consideration of the Brillouin zone sampling. *urn:issn:0567-7394* **1976**, *32*, 259–264.

(3) Baldereschi, A. Mean-Value Point in the Brillouin Zone. *Physical Review B* **1973**, *7*, 5212.

(4) Cunningham, S. L. Special points in the two-dimensional Brillouin zone. *Physical Review B* **1974**, *10*, 4988.

(5) GILAT, G., *Methods of Brillouin Zone Integration*; Elsevier: 1976; Vol. 15, pp 317–370.

(6) Kroon, P. A.; Vos, A. Convergence of Brillouin zone summations. *urn:issn:0567-7394* **1978**, *34*, 823–824.

(7) Monkhorst, H. J.; Pack, J. D. Special points for Brillouin-zone integrations. *Physical Review B* **1976**, *13*, 5188.

(8) Wisesa, P.; McGill, K. A.; Mueller, T. Efficient generation of generalized Monkhorst-Pack grids through the use of informatics. *Physical Review B* **2016**, *93*, 155109.

(9) Sato, S. A. Two-step Brillouin zone sampling for efficient computation of electron dynamics in solids. *Journal of Physics: Condensed Matter* **2021**, *34*, 095903.

CHAPTER 4

VARIATIONAL 2-ELECTRON REDUCED DENSITY MATRIX METHODS

4.1 From wavefunctions to RDMs

Because the Hamiltonian only includes one-body and two-body interactions, we can use second quantization to expand the hamiltonian[1] in a two-body basis as:

$$\hat{H} = \frac{1}{2}\sum_{ijkl} H_{ijkl}\hat{a}_i^\dagger \hat{a}_j^\dagger \hat{a}_l \hat{a}_k \tag{4.1}$$

where $\hat{a}_i^\dagger$ and $\hat{a}_i$ are fermionic creation and annihilation operators, respectively, defined as

$$\hat{a}_i|\Psi\rangle = \int \phi_i(N)\Psi(1,2,\ldots,N)dN \tag{4.2}$$

$$\hat{a}_i^\dagger|\Psi\rangle = |\phi_i\rangle \wedge |\Psi\rangle \tag{4.3}$$

Using second quantization, then, we can rewrite the Schrödinger equation in Eq. 1.1 without approximation as

$$E = \sum_{ijkl} H_{ijkl}{}^2D_{ijkl} = \mathrm{Tr}(H^2D) \tag{4.4}$$

where ${}^2D$ is the 2-electron Reduced Density Matrix (2-RDM), defined as

$${}^2D_{ijkl} = \frac{1}{2}\langle\Psi_n|\hat{a}_i^\dagger \hat{a}_j^\dagger \hat{a}_l \hat{a}_k|\Psi_n\rangle \tag{4.5}$$

Therefore we have converted the typical Schrödinger equation, for which the form of the wavefunction is the primary independent variable, to a form where the 2-RDM is the primary variable. In this transformation we make no approximations, but we impose a basis

set which transforms the real-space many-electron problem to a matrix equation within the given basis set. Although this result is exact when using a complete basis set, in practice approximately complete basis sets are used which add a degree of approximation the state of the system. We'll discuss this more in the next section.

4.2 Computational Scaling and FCI Configuration Truncation

This transformation from using a wavefunction as the basic variable to using a 2-RDM as the basic variable can reduce the computational complexity of some post-Hartree Fock methods. For example, the Full Configuration Interaction (FCI) method treats correlation exactly within a given basis set by defining the N-electron wavefunction as a linear combination of all possible excitations from a reference wavefunction. However, the number of excitations increases exponentially with the number of basis functions, and therefore computational cost increases exponentially and quickly becomes prohibitively expensive. By contrast, the number of elements in the 2-RDM increases as r^4 where r is the basis set size, and therefore methods which exploit the 2-RDM can attain polynomial scaling.

Due to the exponential scaling of the FCI method, the electronic configurations are often truncated according to an ansatz to approximate the FCI wavefunction with fewer configurations. In a singlet system with N electrons and r spatial orbitals, denoted as an $[N, r]$ system, there are a total of the binomial coefficient $\binom{r}{N/2}^2$ FCI configurations that preserve spin-symmetry. For example, a [4,4] system has 36 total configurations whereas an [8,8] system has 4900. There are several commonly used methods for truncating the set of configurations, such as Configuration Interaction (CI) with single and double excitations (CISD),[2] CI with double excitations (CID), and complete active space CI (CASCI) methods.[3–6]

CISD configurations are chosen such that all configurations are obtained via a single or double excitation from a reference state. As an example, the 5th configuration in Fig. 4.1 would be included in a CISD calculation (assuming the ground state reference) but the 7th

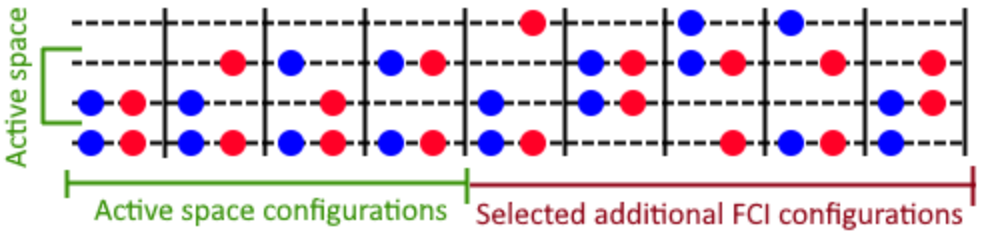

Figure 4.1: Schematic depiction of the active space configuration truncation. Blue and red circles correspond to spin-up and spin-down electrons, with dashed horizontal lines corresponding to different energy levels in a system with 4 electrons and 4 energy states. There are 36 FCI configurations, but only those contributing to a [2,2] active space and a few selected additional configurations are shown.

configuration would not, because three electrons have been excited from the reference state. For a [4,4] system, the 36 total configurations are reduced to 27 CISD configurations, and the computational benefit grows as the system increases in size, as there are more configurations obtained through higher excitations.

By contrast, active space calculations divide the molecular orbitals into core (occupied), active, and virtual (unoccupied) orbitals. Only configurations which keep the core orbitals occupied and virtual orbitals unoccupied are included in complete active space calculations. Therefore, active space calculations effectively solve the FCI problem on a subset of electrons and orbitals in the system, and we can choose the number of orbitals and electrons to best suit the chemistry of the system. In our [4,4] example system, we can select the 2nd and 3rd orbitals as well as 2 electrons for our active space, essentially solving a [2,2] FCI problem which only has 4 configurations (see Fig. 4.1). However, because the configurations can be chosen explicitly to be the chemically relevant, configurations in active space calculations generally have a higher contribution to the wavefunction than other configurations.

Additionally, we can perform an orbital rotation procedure after each individual CASCI calculation, and self-consistently minimize the energy by repeating the CASCI calculation. This procedure is called CASSCF, and it reduces the dependence on the initial choice of orbitals by rotating contributions from the remaining orbitals into the active space with

each SCF step.

4.3 Constrained Optimization

However, the use of the 2-RDM as the basic variable comes with additional complications compared to wavefunction methods. Simply minimizing the energy in Eq. 4.4 by varying 2-RDM elements produces an energy that is too low, because not all matrices represent a physical N-electron wavefunction. The necessary conditions for the 2-RDM to represent at least one N-electron wavefunction are called N-representability conditions,[7–9] and they can be assembled into a heirarchy of p-positivity conditions.[10] The 1-positivity conditions require the 1-RDM and the 1-hole matrices be positive semidefinite:

$$^1D \succeq 0 \tag{4.6}$$

$$^1Q = I - {}^1D \succeq 0 \tag{4.7}$$

These conditions are often summarized as Pauli's exclusion principle, which states that no two electrons can have the same quantum numbers, or equivalently that the eigenvalues of the 1-RDM are between 0 and 1. Similarly, the 2-positivity conditions require the 2-RDM, the 2-hole matrix, and the particle-hole matrix to be positive semidefinite. Like the 1-RDM and the 1-hole matrices, the 2-hole and the particle-hole matrices are related to the 2-RDM through linear transformations, so all 3 conditions constrain the space of possible 2-RDMs. Similar constraints exist for every $p \leq N$, but it has been shown that the 1-positivity and 2-positivity conditions alone provide reasonable accuracy compared to the FCI limit.[5,11]

To summarize, we can convert the exponential scaling of wavefunction methods with a constrained optimization over 2-RDM elements, for which we can attain polynomial scaling. To perform this optimization, we use a convex optimization technique known as semidefinite programming.[12] Schematically, semidefinite programming in general solves the following

problem:

$$\text{minimize } \mathrm{Tr}(CX) \tag{4.8}$$

$$\text{subject to } \mathrm{Tr}(A_i X) = b_i \tag{4.9}$$

$$\text{where } X \succeq 0 \tag{4.10}$$

Technically this is the *primal* formulation of the semidefinite program in a primal-dual formulation, but the final result is guaranteed to satisfy these conditions (within tolerance), and the dual solution is discussed in-depth elsewhere. In the context of solving the Schrödinger equation, the C matrix is the Hamiltonian, the A matrix and b vector encode the p-positivity conditions, and the X matrix is a block-diagonal matrix of the 2-RDM (^2D), 2-hole matrix (^2Q), and particle-hole matrix (^2G):

$$X = \begin{bmatrix} {}^2D & 0 & 0 \\ 0 & {}^2Q & 0 \\ 0 & 0 & {}^2G \end{bmatrix} \tag{4.11}$$

Because we're minimizing the energy of the system through the semidefinite program formulation of the Schrödinger equation, we call this optimization method the Variational 2-electron Reduced Density Matrix (v2RDM) method.

4.4 Applications to Periodic Systems

As suggested by Equation 4.4, the independent variables in the v2RDM method are the matrix elements of the 1-body and 2-body electron integrals. Therefore, when applying the v2RDM method to periodic systems, we only need to address the electron integrals in a manner that is consistent with the periodic boundary conditions. There are additional topics

to be address such as choice of basis, which affect computational efficiency, but the electron integrals are the only necessary change to compute the electronic structure of periodic systems.

For gamma-point calculations, the electron integrals are real-valued, meaning that only the magnitude of the electron integrals changes when the basis functions are adapted to encode the periodic boundary conditions through the Bloch theorem. Therefore, there is no functional difference in the v2RDM algorithm to compute gamma-point calculations - we simply need to compute the electron integrals in the gamma-point basis, and carefully account for the lattice energy after the calculation has finished.

By contrast, the electron integrals for fully k-sampled calculations are naively complex-valued. Due to limitations in the implementation of the SDP solver used for v2RDM, we have to convert the complex-valued SDP into an equivalent real-valued problem, either through a change of basis or through the encoding of complex numbers as matrices. Direct transformation requires use of the mapping from complex numbers to a matrix:

$$a + bi = \begin{bmatrix} a & -b \\ b & a \end{bmatrix} \tag{4.12}$$

Applying this transformation directly to each matrix in the X matrix doubles the size of each block by splitting the real and imaginary parts of each matrix element to the 2x2 matrix above. After the SDP converges, the real and imaginary components of the real-valued SDP can then be extracted and converted back into complex RDMs.

In Chapter 3 we discussed several methods for choosing a basis to "realize" the complex integrals that arise in periodic calculations. By contrast to the matrix form of complex numbers above, these basis adaptation methods assume time-reversal symmetry to avoid doubling the size of the problem. The k-adapted transformation instead doubles the size of each block of 1-electron integrals while keeping the total number of basis functions the

same, and the gamma-point transformation enables a comparison between gamma-point and k-point calculations. However in both cases, the blocking structure of the 2-electron integrals in the k-point basis is lost. Despite the conservation of momentum which causes the block structure in the k-point basis, the mixing of basis vectors of different momenta (even when equal in magnitude) creates a blocked band matrix, where there are additional blocks that act as cross-terms between blocks on the diagonal. This is significant because the blocking structure of the electron integrals is detected by v2RDM and used to solve each block independently from the others, thereby increasing computational speed. As such, it may be preferable to choose the matrix form of complex numbers approach described above, because the additional cost of doubling the size of the calculation could be offset by the efficiency gained through exploiting block structure, especially for calculations with a large number of k-points. Additional work is needed to verify the scaling of this tradeoff.

References

(1) Mayer, I. Towards a "Chemical" Hamiltonian. *International Journal of Quantum Chemistry* **1983**, *23*, 341–363.

(2) Barr, T. L.; Davidson, E. R. Nature of the Configuration-Interaction Method in Ab Initio Calculations. I. Ne Ground State. *Physical Review A* **1970**, *1*, 644.

(3) Roos, B. O.; Taylor, P. R.; Sigbahn, P. E. A complete active space SCF method (CASSCF) using a density matrix formulated super-CI approach. *Chemical Physics* **1980**, *48*, 157–173.

(4) Mazziotti, D. A. Two-Electron Reduced Density Matrix as the Basic Variable in Many-Electron Quantum Chemistry and Physics. *Chemical Reviews* **2011**, *112*, 244–262.

(5) Gidofalvi, G.; Mazziotti, D. A. Active-space two-electron reduced-density-matrix method: Complete active-space calculations without diagonalization of the N -electron Hamiltonian. *Journal of Chemical Physics* **2008**, *129*, 134108.

(6) Veryazov, V.; Malmqvist, P. Å.; Roos, B. O. How to select active space for multiconfigurational quantum chemistry? *International Journal of Quantum Chemistry* **2011**, *111*, 3329–3338.

(7) Mazziotti, D. A.; Erdahl, R. M. Uncertainty relations and reduced density matrices: Mapping many-body quantum mechanics onto four particles. *Physical Review A* **2001**, *63*, 042113.

(8) Mazziotti, D. A. Structure of Fermionic density matrices: Complete N-representability conditions. *Physical Review Letters* **2012**, *108*, 263002.

(9) Mazziotti, D. A. Pure- N -representability conditions of two-fermion reduced density matrices. *Physical Review A* **2016**, *94*, 032516.

(10) Hammond, J. R.; Mazziotti, D. A. Variational two-electron reduced-density-matrix theory: Partial 3-positivity conditions for N-representability. *Physical Review A* **2005**, *71*, 062503.

(11) Hemmatiyan, S.; Mazziotti, D. A. Unraveling the Band Gap Trend in the Narrowest Graphene Nanoribbons from the Spin-Adapted Excited-Spectra Reduced Density Matrix Method. *The Journal of Physical Chemistry C* **2019**, *123*, 14619–14624.

(12) Vandenberghe, L.; Boyd, S. Semidefinite Programming. *Society for Industrial and Applied Mathematics* **1996**, *38*, 49–95.

CHAPTER 5

CORRELATION-DRIVEN PHENOMENA IN PERIODIC MOLECULAR SYSTEMS FROM VARIATIONAL TWO-ELECTRON REDUCED DENSITY MATRIX THEORY

Reprinted with permission from S. Ewing and D. A. Mazziotti, *Journal of Chemical Physics* **154** (2021).

5.1 Abstract

Correlation-driven phenomena in molecular periodic systems are challenging to predict computationally not only because such systems are periodically infinite but also because they are typically strongly correlated. Here we generalize the variational two-electron reduced density matrix (2-RDM) theory to compute the energies and properties of strongly correlated periodic systems. The 2-RDM of the unit cell is directly computed subject to necessary N-representability conditions such that the unit-cell 2-RDM represents at least one N-electron density matrix. Two canonical but non-trivial systems, periodic metallic hydrogen chains and periodic acenes, are treated to demonstrate the methodology. We show that, while single-reference correlation theories do not capture the strong (static) correlation effects in either of these molecular systems, the periodic variational 2-RDM theory predicts the Mott metal-to-insulator transition in the hydrogen chains and the length-dependent polyradical formation in acenes. For both hydrogen chains and acenes the periodic calculations are compared with previous non-periodic calculations with the results showing a significant change in energies and increase in the electron correlation from the periodic boundary conditions. The 2-RDM theory, which allows for much larger active spaces than are traditionally possible, is applicable to studying correlation-driven phenomena in general periodic molecular solids and materials.

5.2 Introduction

Computing the electronic structure of extended molecules and materials can reveal important information such as the band gap, reactivity, and bulk properties such as conductivity or polarizability. As such, accurate methods for computing the electronic structure of materials is of interest to many fields, including the study of inorganic polymers, organic electronics, semiconductors, and superconductors.[1–12] Electronic structure calculations on extended materials are only computationally tractable in cases where periodic boundary conditions can be imposed, which separate the electrons and orbitals into smaller, periodically repeating, unit cells. Commonly used methods for such calculations include density functional theory (DFT),[13–16] GW approximations,[17] quantum Monte Carlo methods,[18] and coupled cluster (CC) theory.[19] Many of these methods, however, have difficulty computing strongly correlated periodic materials with high accuracy at an efficient computational cost, and hence, there is a need for further advances in methods and theories.

Here we present an approach to the calculation of electronic structures for periodic materials in the gamma-point approximation based on the variational calculation of the 2-electron reduced density matrix (2-RDM). In the variational 2-RDM (v2RDM) method,[20–33] the 2-RDM is constrained by N-representability conditions that are necessary for the 2-RDM to represent at least one N-electron density matrix. Because these conditions are necessary, the minimization of the energy with respect to the 2-RDM generates a lower bound on the ground-state energy in the given basis set. Furthermore, because the constraints known as p-positivity conditions restrict the metric matrices of q particles and $(p-q)$ holes to be positive semidefinite,[34,35] the variational 2-RDM method has a well-defined, physical solution even in the presence of strong electron correlation. The 2-positivity conditions, which include the nonnegativity of the particle-particle ${}^2D$, hole-hole ${}^2Q$, and particle-hole ${}^2G$ matrices, have been shown to be capable of describing strongly correlated phenomena including polyradical character in extended conjugated systems,[27,36] ligand non-innocence in transition-metal

complexes,[37,38] non-superexchange mechanisms in bridged transition-metal dimers,[39] and exciton condensation in electron double layers.[12]

Extension of the v2RDM theory to treat periodic boundary conditions allows us to treat the electronic structure of strongly correlated periodic molecules without performing multiple molecular (open boundary condition) calculations and extrapolating to the infinite-length limit. Because the periodic v2RDM method with the 2-positivity conditions only scales as $\mathcal{O}(r^6)$ where r is the number of active orbitals in the unit cell, we can perform calculations with much larger active spaces than possible with traditional methods.[37,40] Through the N-representability conditions the v2RDM theory includes multi-body correlation that are difficult for many traditional periodic methods to capture. Although we present the periodic v2RDM method in the gamma-point approximation here, the formalism can be extended to include k-point sampling. To demonstrate the periodic v2RDM theory, we treat two extended systems, known for exhibiting strong electron correlation: hydrogen chains and acene chains. Both systems are difficult to treat accurately with traditional methods like second-order many-body perturbation theory, configuration interaction with single and double excitations, or coupled cluster theory with single and double excitations extended to periodic boundary conditions. The hydrogen chains undergo a Mott metal-to-insulator transition[41,42] upon dissociation with the insulator phase being strongly correlated, whereas the acene chains become strongly correlated with polyradical character as the lengths of the chains increase.

5.3 Theory

We discuss the v2RDM theory, periodic boundary conditions, and their combination into a periodic v2RDM method.

5.3.1 Variational 2-electron Reduced Density Matrix Methods

The 1-RDM and 2-RDM are defined by integrating the full N-electron density matrix over the spatial and spin coordinates of all but one or two electrons, respectively. Using second quantization, we can represent the elements of the 1- and 2-RDMs as

$$^1D^i_j = \langle\Psi|\hat{a}^\dagger_i\hat{a}_j|\Psi\rangle \tag{5.1}$$

$$^2D^{i,j}_{k,l} = \frac{1}{2}\langle\Psi|\hat{a}^\dagger_i\hat{a}^\dagger_j\hat{a}_l\hat{a}_k|\Psi\rangle \tag{5.2}$$

where $\hat{a}^\dagger_m$ and $\hat{a}_m$ are the second-quantized creation and annihilation operators for spin orbital $|\psi_m\rangle$.[20–23,26,43,44] Notably, the 1-RDM can be derived from the 2-RDM by integrating over the spatial and spin coordinates for one of the two electrons. These spin RDMs can be converted into spatial RDMs by tracing over the spin of the electrons. Eigenvalues of spatial 1-RDMs, also known as spatial natural orbital occupation numbers,[45] represent the numbers of electrons in the spatial orbitals, and by the Pauli exclusion principle they are constrained to lie between 0 and 2. A signature of strong correlation, or contributions from multiple Slater determinants, is the presence of fractionally filled orbitals, which are characterized by eigenvalues of the spatial 1-RDM near one.[46] Similarly, eigenvalues of 2-RDMs represent the number of electrons in each two-electron function, known as a geminal, and partially-filled geminals contribute to correlation.

For systems that have at most pairwise interactions, the molecular energy can be written as a functional of the 2-electron reduced density matrix:

$$E = \mathrm{Tr}\left(^1H\,^1D\right) + \mathrm{Tr}\left(^2V\,^2D\right) \tag{5.3}$$

where ^1H and ^2V are the reduced Hamiltonian matrices of the 1-electron and 2-electron integrals. The variational 2-RDM (v2RDM) method minimizes the ground-state energy in

Eq. 5.3, with the 2-RDM as the fundamental variable rather than the wavefunction.[22,24,47] Often, the v2RDM method is combined with the notion of an active space, a set of orbitals that are correlated in a mean field of the remaining orbitals.[27,48] A system where n electrons are allowed to fill r spatial orbitals is denoted an $[n, r]$ active space. If n is equal to the total number of electrons and r is equal to the size of the basis set, then the calculation approximates the energies from full configuration interaction (FCI).

Central to RDM calculations is the concept of N-representability, which requires that an RDM represents a physical N-electron density matrix.[35,43,49] The simplest and most familiar N-representability constraint is the Pauli exclusion principle, which states that eigenvalues of the spatial 1-RDM must lie between 0 and 2. Similar constraints exist for the 2-electron RDM, the particle-hole RDM (${}^2G$), and the 2-hole RDM (${}^2Q$), namely ${}^2D \succeq 0$, ${}^2G \succeq 0$, and ${}^2Q \succeq 0$, restricting the eigenvalues of all three matrices to be non-negative. All three of these constraints restrict the space of valid 2-RDMs because ${}^2G$ and ${}^2Q$ are related by linear mappings to the 2-RDM.[22] Minimizing the energy from a 2-RDM subject to these constraints generates an optimization problem known as a semidefinite program.[47,50–52] The solution of the semidefinite program yields a lower bound to the ground-state energy from a complete active space configuration interaction (CASCI) calculation[48] but with a computational scaling that is polynomial in the size of the active space.

5.3.2 Periodic Boundary Conditions

For molecules with extended structures, additional symmetries must be exploited to make accurate electronic structure calculations tractable. Calculations on periodic molecules can be altered to account for the periodic boundary conditions (PBCs) of the molecule by using periodic basis functions. Bloch waves are the simplest way to construct a complete basis set of periodic functions, but the underlying structure for these basis functions can vary, and are usually chosen to be either Gaussian[53,54] or plane waves.[55–58] In general, Bloch waves

can be defined as

$$|\Psi_k(r)\rangle = e^{ik\cdot r}u(r) \tag{5.4}$$

where $u(r)$ is a function for which the periodic boundary conditions are satisfied and k is a momentum vector. For many cases, the gamma point, where only $k = 0$ wave vectors are included in the basis set, gives an accurate approximation to the complete basis while greatly simplifying the computational complexity. Although plane waves automatically satisfy the periodic boundary conditions, they do not resolve atomic details as readily as Gaussian basis functions. In the case of Gaussian functions periodic boundary conditions can be imposed through a local basis approximation:[54]

$$|\Psi_k(r)\rangle = \sum_T e^{ik\cdot T}u(r-T) \tag{5.5}$$

where T is a lattice translational vector, and $u(r-T)$ is a local Gaussian atomic basis function. This approximation accounts for periodicity by summing over images of each basis function in neighboring cells. As the number of translational vectors in the sum over T increases, the wavefunction will more closely approach the periodic boundary conditions, because the closest cells are being explicitly included. Once the basis set is chosen to satisfy the boundary conditions, the 1-electron and 2-electron integral matrices can be computed and used in the v2RDM method. We use the PySCF built-in integration methods to evaluate these integrals using the local basis approximation.[54]

Without the use of periodic boundary conditions, extended systems are typically approximated by computing molecular systems of varying sizes and extrapolating to the infinite limit. In this form of analysis, several assumptions are made about the energy density of the system so that the energies of the different systems can be subtracted, leaving an "effectively edgeless" system. Namely, it is assumed that the system is long enough that the system can be broken into several classes of edge subsystems and edgeless (quasi-periodic) subsystems.

By subtracting the energy of smaller systems that contain no (or fewer) edgeless subsystems, the energy of the central systems can be approximated. However, gamma point calculations compute these systems directly due to the PBCs used in the unit cell, and these calculations are often much cheaper because there is no need to compute the electronic structure of a supercell. Additionally, we posit that gamma point calculations better represent the extended systems than molecular calculations of the same size, for two main reasons: first, molecular calculations typically require several calculations to get an energy so that the analysis above can be performed. Second, periodic calculations eliminate the computational time and power needed to compute the electronic structure of the edge subsystems, which are ultimately discarded. Additionally, this discarding of data unnecessarily complicates the analysis of these computations for obervables other than the energy.

In both forms of analysis, the assumption that the (quasi) periodic unit cells are identical - no phase change between cells - can be relaxed to get a more accurate representation of the extended structure, since long-range order can affect the electronic structure in extended systems. For molecular calculations, the analysis above is simply extended further to larger systems, which reduces the inaccuracy due to each approximation. Using PBCs, there are two main methods for relaxing this assumption: including k-points or including more repeating units in the unit cell. Including k-points explicitly adds basis functions that allow for phase changes between unit cells. Similarly, including more repeating units in the unit cell allows the wavefunction to change phase between repeating units within the cell. The results of a gamma point calculation with N repeated units in the unit cell can be shown to be equivalent to a k-point calculation on a single unit cell with N k-points, because the volume of the Brillouin zone is inversely proportional to the volume of the unit cell. The main motivation for k-point calculations is to exploit translational symmetry to decrease computation time, which is the subject of future work for this method.

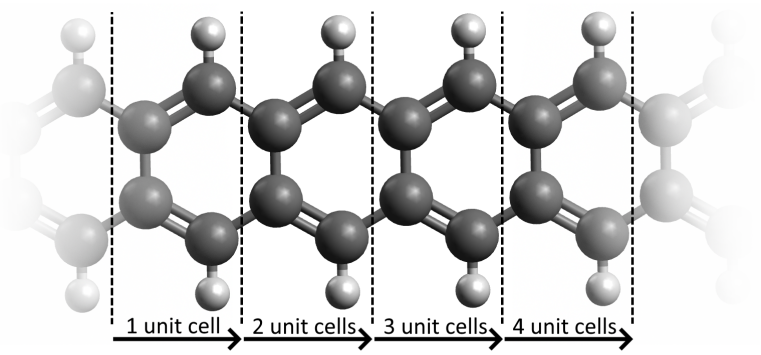

Figure 5.1: The acene chain systems used for calculations have various numbers of repetitions of the unit cell inside one periodic box. Every unit cell contains 4 carbon atoms and 2 H atoms, for a total of 26 electrons and 40 orbitals in the 6-31G basis set. Of those orbitals, 4 electrons and 4 orbitals ([4,4] active space) were used from each unit cell in the active space calculations.

5.4 Results

5.4.1 Methods

Hydrogen chain symmetric dissociation curves were computed with H_{10} in the unit cell, using the correlation-consistent polarized valence double-zeta (cc-pVDZ)[59] basis set. Both molecular and periodic calculations were completed in a [10,20] active space. Additional calculations were performed using DFT (B3LYP functional), configuration interaction with single and double excitations (CISD), and Møller-Plesset 2nd-order perturbation theory (MP2)[60] methods. Each of these calculations were performed using the implementations in PySCF.[54,61]

Additionally, the electronic structure of acene chains were computed using the periodic v2RDM method and the 6-31g basis set, with crystal structure coordinates obtained from the American Mineralogist Crystal Structure Database.[62] A series of calculations were performed, with 1-10 repetitions of the unit cell inside the periodic box. For each calculation, we used a [4,4] active space per repeated unit, which accounts for the complete π-space. Therefore, the 10-unit calculation had an active space of [40,40]. This procedure ensured that the energy per repeated unit and occupation numbers were converged, and revealed

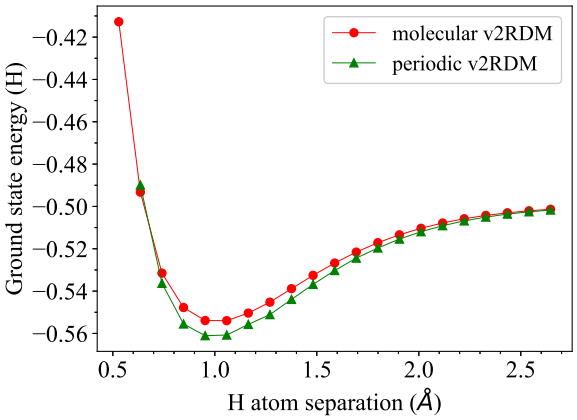

Figure 5.2: Dissociation curves for H_{10}, using molecular v2RDM and periodic v2RDM with a [10,20] active space and the cc-pVDZ basis set. Results agree with previous data,[63,64] showing the equilibrium bond length at 0.95-1.05 Å.

information about the parity of the periodic orbitals. The occupation numbers from periodic v2RDM were then compared to those obtained via gamma-point calculations using PySCF-builtin periodic coupled cluster methods.[54] Finally, the energy, natural orbital (NO) occupation numbers, and several forms of entropy were computed for molecular acene chains with 2, 4, 6, and 8 rings, using the v2RDM method. The molecular calculations had active spaces of [10,10], [18,18], [26,26], and [34,34], respectively, corresponding once again to the full π-space. Geometries for these molecular chains were obtained from the supplementary data from Ref..[2] These results are compared to the calculations using the periodic method.

5.4.2 Hydrogen Chain

Previous work on the extended hydrogen chain has focused on obtaining the dissociation curve through various extrapolation techniques, starting from molecular calculations.[64,65] Molecular energies for multiple chain lengths are calculated, and then compared with each other to extrapolate to the infinite chain length, or the thermodynamic, limit. We use the PBC approach to compute the ground state energy of the hydrogen chain, which removes the edge effects entirely without extrapolation.

Examining the dissociation curve for H_{10} in Fig. 5.2 we observe that the molecular and periodic systems converge to the same energy, around 5 hartrees, as the spacing between hydrogen atoms increases. In this regime, the hydrogen atoms begin to behave independently, so the total energy is approximately 10 times the energy of a single hydrogen atom. However, interesting differences develop as the separation distance decreases. The equilibrium bond length lies at 0.95-1.05 Å, and the periodic system has a deeper well by 6.6 millihartrees per atom. This agrees with previous work by Motta *et al.*[64] that indicates through extrapolating molecular calculations to the infinite limit that the periodic system has a deeper well by about 4 millihartrees per atom.

One metric that has been used[66–68] to discuss the Mott metal-to-insulator transition is the sum of the magnitudes of the off-diagonal elements of the 1-RDM in the atomic orbital basis, denoted γ. Because the metal-to-insulator transition is a long-range effect, we ignore elements corresponding to orbitals on a single atom, instead summing over the off-diagonal elements that correspond to electron density shared between atoms. We add these elements of the 1-RDM in quadrature, as a parallel to the Frobenius norm of the matrix. See the Supporting Information for additional details. When the system has long-range order, this metric will be large, indicating strong metallic behaviour, and when the system has no long-range order, this metric will be small, indicating strong insulating behaviour. Fig. 5.3 shows the metric as a function of the atomic spacing in H_{10}. The Mott transition metric for periodic Hartree-Fock calculations is nearly constant for all bond lengths. A similar absence of the transition to an insulator is seen from the DFT with the B3LYP functional, MP2, and CISD (As observed in previous work,[51] the coupled cluster calculations with single and double excitations do not converge far beyond the equilibrium bond length, and hence, it is not included in the reported data). By contrast, the periodic v2RDM calculations exhibit the expected transition from metallic to insulating properties as the bond length increases.

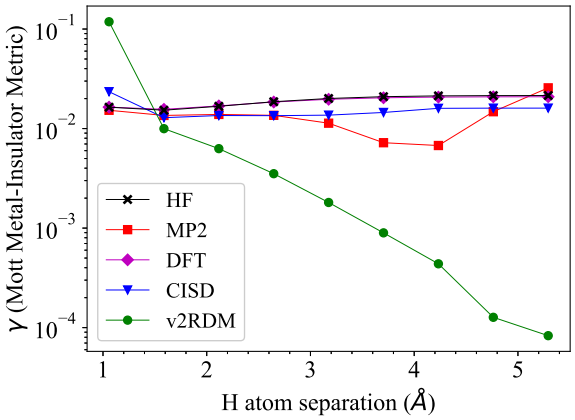

Figure 5.3: Mott metal-to-insulator metric as a function of hydrogen atom spacing for H_{10}, for various periodic methods. Hartree-Fock and other post-Hartree-Fock calculations produce a metric that is relatively constant across all bond lengths, whereas both molecular[66] and periodic v2RDM calculations have an appropriate transition from metal to insulator as the bond length increases.

5.4.3 Acene Chain

NO occupations for periodic calculations are shown in Table 5.1 and Figure 5.4, which show that the known polyradical nature[69–71] of acene chains is only recovered by v2RDM for periodic boxes with an even number of unit cells included. The coupled cluster singles-doubles (CCSD) method with periodic boundary conditions only recovers static correlation in the 2 unit cell case. Notably, the CCSD calculation does not exhibit significant static correlation in the 4 unit cell case. Multi-reference wavefunctions are needed to accurately capture static correlation, and CCSD, a single-reference method, fails to accurately capture static correlation in larger systems. This result is consistent with previous limitations with CCSD observed in the computation of finite acene chains.[27] The highest-occupied natural orbitals (HONOs) and lowest-unoccupied natural orbitals (LUNOs) that display biradical character have a 180° phase change between unit cells (see Figure 5.5), which explains the requirement for an even number of unit cells to achieve the biradical character. This also agrees with previous molecular (non-periodic) calculations suggesting this same parity.[36]

	Natural Orbital Occupation Numbers							
	1 unit cell		2 unit cells		3 unit cells		4 unit cells	
	CCSD	v2RDM	CCSD	v2RDM	CCSD	v2RDM	CCSD	v2RDM
HONO-2	1.9594	-	1.9082	1.9036	1.9361	1.9321	1.8992	1.8662
HONO-1	1.9580	1.9842	1.9055	1.8918	1.9032	1.8515	1.8992	1.8662
HONO	1.9440	1.9743	1.4740	1.3558	1.9032	1.8515	1.7194	1.3479
LUNO	0.0475	0.0263	0.5215	0.6457	0.0902	0.1511	0.2782	0.6597
LUNO+1	0.0391	0.0152	0.0845	0.1109	0.0902	0.1511	0.0922	0.1309
LUNO+2	0.0301	-	0.0841	0.0943	0.0548	0.0688	0.0922	0.1309

Table 5.1: Natural orbital occupations for acene chains with 1-4 unit cells in the periodic box. v2RDM calculations show strong correlation for even numbers of unit cells, whereas CCSD fails to recover strong correlation except in the 2 unit cell calculation. CCSD calculations were only performed up to 4 unit cells due to the expensive memory requirements for longer chains.

Although one unit cell contains only 4 carbon atoms and 2 hydrogen atoms, gamma-point calculations should be performed on a box containing two unit cells to accurately reflect molecular properties.

Electron densities for 8 ring molecular, 8-unit periodic, and 9-unit periodic calculations are included in Figure 5.5. These images show clearly that the HONO-1 and LUNO+1 orbitals from the molecular calculation have even parity, while the HONO and LUNO have odd parity. Additionally, the electron density of the even parity orbitals remain unchanged in the 8-unit periodic calculation, and the odd parity orbitals remain unchanged in the 9-unit periodic calculation (after translation along the periodic axis). As a result, the occupations of the HONO and LUNO closely match those in the 9-unit periodic calculation, whereas the HONO-1 and LUNO+1 orbital occupations closely match those in the 8-unit periodic calculation (shown in Figure 5.4). Notably, each orbital in the 9-unit periodic calculation has a single "defect" which looks like the electron density along the edge of the molecular calculation. Because there are an odd number of repeating units in the unit cell, and gamma point calculations can only recover orbitals with an even number of antinodes, the defects effectively stretch an even number of antinodes across the unit cell. Finally, the symmetry of the 8-unit periodic calculation HONO and LUNO explain the early convergence of the

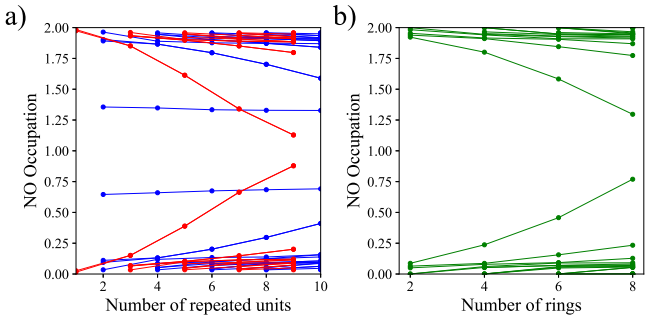

Figure 5.4: NO occupations for periodic (a) and molecular (b) acene chain calculations. In (a), the even-unit calculations are colored blue and the odd-unit calculations are colored red, to emphasize the differences in occupation trends between the two sets of calculations. Notably, the odd-unit calculations have a similar HONO and LUNO occupation trend as the molecular calculations, whereas the even-unit calculations have the same HONO and LUNO occupations across all calculations.

occupation. Since these orbitals are just 4 copies of the 2-antinode pattern fully contained in 2 repeated units, these orbitals in particular stay the same for any even number of repeated units in the unit cell.

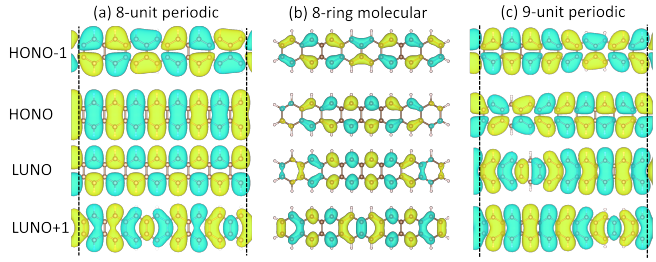

Figure 5.5: Images of electron density for HONO-1, HONO, LUNO, and LUNO+1 for molecular (8-acene, (a)) and periodic (8-unit, (b), and 9-unit, (c)) calculations. The dashed lines in the structures for the periodic calculations represent the lattice boundary.

Earlier results using molecular DMRG[2] also indicate the polyradical behaviour of acene chains, but significant static correlation is only recovered for chain lengths longer than 6 rings, and the partial occupation levels only reach the values obtained here (1.35 HONO and 0.66 LUNO occupations for 6 unit cells) for chain lengths of 10 rings. Thus, we conclude that this periodic v2RDM method accurately captures strong correlation efficiently compared to DMRG methods, in that fewer atoms and orbitals are needed to observe strong correlation

effects. Additionally, this method is generalizable to 2- or 3- dimensional systems (by summing over neighboring cells in 2 or 3 axes in Equation 5.5), whereas DMRG methods are typically restricted to 1-dimensional systems.

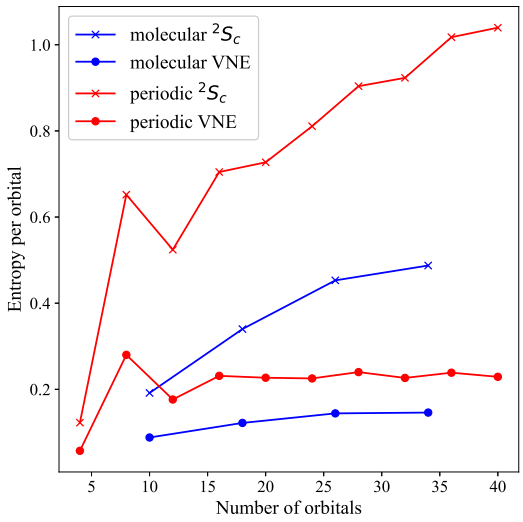

Figure 5.6: 1-electron Von Neumann entropy and connected entropy (^2S_c) of molecular and periodic acene chains of various lengths. Periodic calculations have active spaces of $[4n, 4n]$ where n is the number of repeated units in the unit cell, and molecular calculations have active spaces of $[4n+2, 4n+2]$ where n is the number of rings in the calculation. The entropy of each calculation has been divided by the number of orbitals to get an intensive entropy measure that can be compared directly between calculations.

For the both the periodic and molecular acene calculations, we include the 1-electron Von Neumann Entropy (1-VNE) and a 2-electron form of entropy of quantum entropy (we call the connected entropy) originally created by Prezhdo[72] in Figure 5.6. The connected entropy is defined as:

$$^2S_c = NS(^1D) - S(^2D) \tag{5.6}$$

where N is the number of electrons and $S(M) = -\mathrm{Tr}(M \ln M)$ is the Von Neumann entropy. Both the 1-VNE and the connected entropy are extensive, and the 1-VNE quantifies the amount of bipartite correlation whereas the connected entropy quantifies the amount of

tripartite correlation in the system. To compare these quantities between calculations, we divide each by the number of orbitals in the calculation to compare the intensive forms of the entropy. Because the all calculations performed use the complete π-space, these intensive quantities are directly comparable.

The intensive VNE is relatively constant for both molecular and periodic calculations, indicating that bipartite correlation is not increasing, despite the increase in correlation as longer chains are considered. In contrast, the connected entropy increases steadily as chain length increases, indicating an increase in tripartite correlation. Additionally, the periodic calculations have more of each type of entropy than the molecular calculations, for all chain lengths. As a result, the 2-unit periodic calculation recovers more correlation than any molecular calculation performed, which emphasizes the importance of including periodic boundary conditions to capture static correlation in extended systems.

5.5 Discussion and Conclusions

We have generalized the variational 2-electron reduced density matrix (v2RDM) electronic structure theory, which incorporates periodic boundary conditions for extended structures. Using periodic boundary conditions can greatly simplify the computational complexity and accuracy of calculations by removing edge effects. Even gamma-point calculations, for which the electronic structure repeats with no phase change between unit cells, and therefore, does not account for long-range or low-frequency contributions to the wavefunction, can recover a large proportion of the correlation due to periodicity. The proposed periodic v2RDM method was shown to account for a large degree of static correlation due to the multireference nature of 2-RDMs and to correlate electrons between periodic cells. The ability to capture strong correlation in extended structures will prove beneficial in the study of many systems, including systems with extended π-systems, inorganic polymers, and materials, among others.

Additionally, we have confirmed previous work regarding the equilibrium bond length of

the extended hydrogen chain. This is significant because we can efficiently recover an accurate estimate for the ground-state energy of the hydrogen chain system without performing expensive calculations with different chain lengths. We also showed that the periodic v2RDM method can capture the metal-to-insulator transition for the hydrogen chain, which Hartree-Fock, MP2, CISD, and CCSD calculations are unable to do. The success of the v2RDM method is due to its accurate treatment of the strong correlation upon dissociation and its correct description of the periodic nature of the wavefunction. With the application of this method to the acene chain, we have shown that parity effects require that two crystallographic unit cells are used for gamma-point electronic structure calculations.

Due to the ability to represent multireference systems, the 2-RDM methods can accurately capture strongly correlated phenomena in materials without the exponential scaling of full configuration interaction, allowing the use of much larger active spaces than traditionally possible for such systems. The combination of these attributes has the potential for more realistic descriptions of correlation-driven phenomena in extended π-systems, semiconductors, superconductors, organometallic polymers, as well as other materials.

References

(1) André, J. M.; Vercauteren, D. P.; Bodart, V. P.; Fripiat, J. G. Ab initio calculations of the electronic structure of helical polymers. *Journal of Computational Chemistry* **1984**, *5*, 535–547.

(2) Hachmann, J.; Dorando, J. J.; Avíls, M.; Chan, G. K. L. The radical character of the acenes: A density matrix renormalization group study. *Journal of Chemical Physics* **2007**, *127*, 134309.

(3) Dimitrakopoulos, C.; Malenfant, P. Organic Thin Film Transistors for Large Area Electronics. *Advanced Materials* **2002**, *14*, 99–117.

(4) Reese, C.; Roberts, M.; Ling, M. M.; Bao, Z. Organic thin film transistors. *Materials Today* **2004**, *7*, 20–27.

(5) Chen, L.; Batra, R.; Ranganathan, R.; Sotzing, G.; Cao, Y.; Ramprasad, R. Electronic Structure of Polymer Dielectrics: The Role of Chemical and Morphological Complexity. *Chemistry of Materials* **2018**, *30*, 7699–7706.

(6) Kaewmeechai, C.; Laosiritaworn, Y.; Jaroenjittichai, A. P. Electronic structure of nontoxic-inorganic perovskite: CsMgBr3 using DFT calculation - IOPscience. *Journal of Physics: Conference Series* **2019**, *1380*.

(7) Kim, J. Band Structure Calculations of Strained Semiconductors Using Empirical Pseudopotential Theory, 2011.

(8) Zerveas, G. et al. Comprehensive comparison and experimental validation of band-structure calculation methods in III-V semiconductor quantum wells. *Solid-State Electronics* **2016**, *115*, 92–102.

(9) Xie, J.; Boyn, J. N.; Filatov, A. S.; McNeece, A. J.; Mazziotti, D. A.; Anderson, J. S. Redox, transmetalation, and stacking properties of tetrathiafulvalene-2,3,6,7-tetrathiolate bridged tin, nickel, and palladium compounds. *Chemical Science* **2020**, *11*, 1066–1078.

(10) Benayad, N.; Djermouni, M.; Zaoui, A. Electronic structure of new superconductor La0.5Th0.5OBiS2: DFT study. *Computational Condensed Matter* **2014**, *1*, 19–25.

(11) Liu, X.; Zhao, L.; He, S.; He, J.; Liu, D.; Mou, D.; Shen, B.; Hu, Y.; Huang, J.; Zhou, X. J. Electronic structure and superconductivity of FeSe-related superconductors - IOPscience. *Journal of Physics: Condensed Matter* **2015**, *27*.

(12) Safaei, S.; Mazziotti, D. A. Quantum signature of exciton condensation. *Physical Review B* **2018**, *98*, 045122.

(13) Hohenberg, P.; Kohn, W. Inhomogeneous electron gas. *Physical Review* **1964**, *136*, B864.

(14) Kohn, W.; Sham, L. J. Self-consistent equations including exchange and correlation effects. *Physical Review* **1965**, *140*, A1133.

(15) Enkovaara, J. et al. Electronic structure calculations with GPAW: a real-space implementation of the projector augmented-wave method. *Journal of Physics: Condensed Matter* **2010**, *22*, 253202.

(16) Sundararaman, R.; Arias, T. A. Regularization of the Coulomb singularity in exact exchange by Wigner-Seitz truncated interactions: Towards chemical accuracy in nontrivial systems. *Physical Review B* **2013**, *87*, 165122.

(17) Hedin, L. New Method for Calculating the One-Particle Green's Function with Application to the Electron-Gas Problem. *Phys. Rev.* **1965**, *139*, A796.

(18) Caffarel, M.; Claverie, P. Development of a pure diffusion quantum Monte Carlo method using a full generalized Feynman-Kac formula. I. Formalism. *The Journal of Chemical Physics* **1988**, *88*, 1088.

(19) Coester, F. Bound states of a many-particle system. *Nuclear Physics* **1958**, *7*, 421–424.

(20) McWeeny, R. Some Recent Advances in Density Matrix Theory. *Reviews of Modern Physics* **1960**, *32*, 335–369.

(21) Nakata, M.; Nakatsuji, H.; Ehara, M.; Fukuda, M.; Nakata, K.; Fujisawa, K. Variational calculations of fermion second-order reduced density matrices be semidefinite programming algorithm. *Journal of Chemical Physics* **2001**, *114*, 8282–8292.

(22) Mazziotti, D. A. Variational minimization of atomic and molecular ground-state energies via the two-particle reduced density matrix. *Phys. Rev. A* **2002**, *65*, 62511.

(23) Zhao, Z.; Braams, B. J.; Fukuda, M.; Overton, M. L.; Percus, J. K. The reduced density matrix method for electronic structure calculations and the role of three-index representability conditions. *Journal of Chemical Physics* **2004**, *120*, 2095–2104.

(24) Gidofalvi, G.; Mazziotti, D. A. Spin and symmetry adaptation of the variational two-electron reduced-density-matrix method. *Physical Review A* **2005**, *72*, 052505.

(25) Cancès, E.; Stoltz, G.; Lewin, M. The electronic ground-state energy problem: A new reduced density matrix approach. *Journal of Chemical Physics* **2006**, *125*, 064101.

(26) *Reduced-density-matrix mechanics : with applications to many-electron atoms and molecules*; Mazziotti, D. A., Ed.; John Wiley and Sons, Inc.: Hoboken, NJ: 2007.

(27) Gidofalvi, G.; Mazziotti, D. A. Active-space two-electron reduced-density-matrix method: Complete active-space calculations without diagonalization of the N -electron Hamiltonian. *Journal of Chemical Physics* **2008**, *129*, 134108.

(28) Greenman, L.; Mazziotti, D. A. Strong electron correlation in the decomposition reaction of dioxetanone with implications for firefly bioluminescence. *Journal of Chemical Physics* **2010**, *133*, 164110.

(29) Shenvi, N.; Izmaylov, A. F. Active-space N-representability constraints for variational two-particle reduced density matrix calculations. *Physical Review Letters* **2010**, *105*, 213003.

(30) Verstichel, B.; Aggelen, H. V.; Poelmans, W.; Neck, D. V. Variational two-particle density matrix calculation for the hubbard model below half filling using spin-adapted lifting conditions. *Physical Review Letters* **2012**, *108*, DOI: 10.1103/PhysRevLett.108.213001.

(31) Mazziotti, D. A. Two-electron reduced density matrix as the basic variable in many-electron quantum chemistry and physics. *Chemical Reviews* **2012**, *112*, 244–262.

(32) Mazziotti, D. A. Enhanced Constraints for Accurate Lower Bounds on Many-Electron Quantum Energies from Variational Two-Electron Reduced Density Matrix Theory. *Physical Review Letters* **2016**, *117*, DOI: 10.1103/PhysRevLett.117.153001.

(33) Fosso-Tande, J.; Nguyen, T.-S.; Gidofalvi, G.; DePrince, A. E. Large-Scale Variational Two-Electron Reduced-Density-Matrix-Driven Complete Active Space Self-Consistent Field Methods. *Journal of Chemical Theory and Computation* **2016**, *12*, 2260–2271.

(34) Mazziotti, D. A.; Erdahl, R. M. Uncertainty relations and reduced density matrices: Mapping many-body quantum mechanics onto four particles. *Physical Review A* **2001**, *63*, 042113.

(35) Mazziotti, D. A. Structure of Fermionic density matrices: Complete N-representability conditions. *Physical Review Letters* **2012**, *108*, 263002.

(36) Hemmatiyan, S.; Mazziotti, D. A. Unraveling the Band Gap Trend in the Narrowest Graphene Nanoribbons from the Spin-Adapted Excited-Spectra Reduced Density Matrix Method. *The Journal of Physical Chemistry C* **2019**, *123*, 14619–14624.

(37) Schlimgen, A. W.; Heaps, C. W.; Mazziotti, D. A. Entangled Electrons Foil Synthesis of Elusive Low-Valent Vanadium Oxo Complex. *Journal of Physical Chemistry Letters* **2016**, *7*, 627–631.

(38) McIsaac, A. R.; Mazziotti, D. A. Ligand non-innocence and strong correlation in manganese superoxide dismutase mimics. *Physical Chemistry Chemical Physics* **2017**, *19*, 4656–4660.

(39) Boyn, J. N.; Xie, J.; Anderson, J. S.; Mazziotti, D. A. Entangled Electrons Drive a Non-superexchange Mechanism in a Cobalt Quinoid Dimer Complex. *Journal of Physical Chemistry Letters* **2020**, *11*, 4584–4590.

(40) Montgomery, J. M.; Mazziotti, D. A. Strong Electron Correlation in Nitrogenase Cofactor, FeMoco. *J. Phys. Chem. A* **2018**, *122*, 4988–4996.

(41) Bendazzoli, G. L.; Evangelisti, S.; Monari, A. Full-configuration-interaction study of the metal-insulator transition in a model system: Hn linear chains n=4, 6,..., 16. *International Journal of Quantum Chemistry* **2011**, *111*, 3416–3423.

(42) Motta, M. et al. Ground-state properties of the hydrogen chain: insulator-to-metal transition, dimerization, and magnetic phases. **2019**.

(43) Coleman, A. J. Structure of Fermion Density Matrices. *Reviews of Modern Physics* **1963**, *35*, 668–686.

(44) Garrod, C.; Percus, J. K. Reduction of the N-particle variational problem. *Journal of Mathematical Physics* **1964**, *5*, 1756–1776.

(45) Löwdin, P. O.; Shull, H. Natural orbitals in the quantum theory of two-electron systems. *Physical Review* **1956**, *101*, 1730–1739.

(46) Head-Gordon, M. Characterizing unpaired electrons from the one-particle density matrix. *Chemical Physics Letters* **2003**, *372*, 508–511.

(47) Mazziotti, D. A. Large-scale semidefinite programming for many-electron quantum mechanics. *Physical Review Letters* **2011**, *106*, 083001.

(48) Roos, B. O.; Taylor, P. R.; Sigbahn, P. E. A complete active space SCF method (CASSCF) using a density matrix formulated super-CI approach. *Chemical Physics* **1980**, *48*, 157–173.

(49) Mazziotti, D. A. Variational reduced-density-matrix method using three-particle N -representability conditions with application to many-electron molecules. *Physical Review A* **2006**, *74*, 032501.

(50) Vandenberghe, L.; Boyd, S. Semidefinite Programming. *Society for Industrial and Applied Mathematics* **1996**, *38*, 49–95.

(51) Mazziotti, D. A. Realization of quantum chemistry without wave functions through first-order semidefinite programming. *Physical Review Letters* **2004**, *93*, 213001.

(52) Mazziotti, D. A. First-order semidefinite programming for the two-electron treatment of many-electron atoms and molecules. *ESAIM: Mathematical Modelling and Numerical Analysis* **2007**, *41*, 249–259.

(53) Soler, J. M.; Artacho, E.; Gale, J. D.; García, A.; Junquera, J.; Ordejón, P.; Sánchez-Portal, D. The SIESTA method for ab initio order-N materials simulation. *Journal of Physics Condensed Matter* **2002**, *14*, 2745–2779.

(54) Sun, Q.; Berkelbach, T. C.; Blunt, N. S.; Booth, G. H.; Guo, S.; Li, Z.; Liu, J.; McClain, J. D.; Sayfutyarova, E. R.; Sharma, S.; Wouters, S.; Chan, G. K. L. PySCF: the Python-based simulations of chemistry framework. *Wiley Interdisciplinary Reviews: Computational Molecular Science* **2018**, *8*, DOI: `10.1002/wcms.1340`.

(55) Giannozzi, P. et al. QUANTUM ESPRESSO: A modular and open-source software project for quantum simulations of materials. *Journal of Physics Condensed Matter* **2009**, *21*, 395502.

(56) Gonze, X. et al. First-principles computation of material properties: The ABINIT software project. *Computational Materials Science* **2002**, *25*, 478–492.

(57) Kresse, G.; Furthmüller, J. Efficiency of ab-initio total energy calculations for metals and semiconductors using a plane-wave basis set. *Computational Materials Science* **1996**, *6*, 15–50.

(58) Payne, M. C.; Teter, M. P.; Allan, D. C.; Arias, T. A.; Joannopoulos, J. D. Iterative minimization techniques for ab initio total-energy calculations: Molecular dynamics and conjugate gradients. *Reviews of Modern Physics* **1992**, *64*, 1045–1097.

(59) Dunning, T. H. Gaussian basis sets for use in correlated molecular calculations. I. The atoms boron through neon and hydrogen. *J. Chem. Phys* **1989**, *90*, 1007.

(60) Møller, C.; Plesset, M. S. Note on an approximation treatment for many-electron systems. *Physical Review* **1934**, *46*, 618–622.

(61) Sun, Q. et al. Recent developments in the P y SCF program package. *Journal of Chemical Physics* **2020**, *153*, 024109.

(62) Downs, R. T.; Hall-Wallace, M. The American Mineralogist crystal structure database. *American Mineralogist* **2003**, *88*, 247–250.

(63) Stella, L.; Attaccalite, C.; Sorella, S.; Rubio, A. Strong electronic correlation in the hydrogen chain: A variational Monte Carlo study. *Physical Review B* **2011**, *84*, 245117.

(64) Motta, M. et al. Towards the Solution of the Many-Electron Problem in Real Materials: Equation of State of the Hydrogen Chain with State-of-the-Art Many-Body Methods. *Phys. Rev. X* **2017**, *7*, 31059.

(65) Fripiat, J. G.; Dehalle, J.; André, J. M. Electron correlation in linear hydrogen chains. *International Journal of Quantum Chemistry* **1983**, *23*, 1179–1189.

(66) Sinitskiy, A. V.; Greenman, L.; Mazziotti, D. A. Strong correlation in hydrogen chains and lattices using the variational two-electron reduced density matrix method. *Journal of Chemical Physics* **2010**, *133*, 014104.

(67) Smart, S. E.; Mazziotti, D. A. Quantum-classical hybrid algorithm using an error-mitigating N -representability condition to compute the Mott metal-insulator transition. *Physical Review A* **2019**, *100*, 022517.

(68) Tsuchimochi, T.; Scuseria, G. E. Strong correlations via constrained-pairing mean-field theory. *Journal of Chemical Physics* **2009**, *131*, 121102.

(69) Bendikov, M.; Duong, H. M.; Starkey, K.; Houk, K. N.; Carter, E. A.; Wudl, F. Oligoacenes: Theoretical prediction of open-shell singlet diradical ground states. *Journal of the American Chemical Society* **2004**, *126*, 7416–7417.

(70) Jiang, D. E.; Dai, S. Electronic ground state of higher acenes. *Journal of Physical Chemistry A* **2008**, *112*, 332–335.

(71) Ni, Y.; Gopalakrishna, T. Y.; Phan, H.; Herng, T. S.; Wu, S.; Han, Y.; Ding, J.; Wu, J. A Peri-tetracene Diradicaloid: Synthesis and Properties. *Angewandte Chemie - International Edition* **2018**, *57*, 9697–9701.

(72) Luzanov, A. V.; Prezhdo, O. High-order entropy measures and spin-free quantum entanglement for molecular problems. *Molecular Physics* **2007**, *105*, 2879–2891.

CHAPTER 6

CONDUCTIVITY AND BAND STRUCTURE OF AMORPHOUS NITTFTT

Portions of this chapter are included with permission from J. Xie, S. Ewing, J-N. Boyn, B. Cheng, et. al., *Nature*, In review. (2022)

6.1 Abstract

Conducting organic materials underpin many important technologies. These materials must typically be doped to conduct electricity, and metallic behavior requires significant crystallinity. However, engendering undoped intrinsic charge transport in amorphous organic materials provides advantages for processability and durability. Here we show that a tetrathiafulvalene based coordination polymer is completely amorphous but highly conductive(1280 S/cm). Characterization suggests metallic behavior, and advanced theoretical analysis suggests that molecular overlap that is robust to structural distortions is the origin of high conductivity. This unusual combination of intrinsic metallic charge transport and disorder results in a high degree of thermal and aerobic stability. Our results demonstrate that molecular design can enable metallic conductivity even in heavily disordered organic materials. This raises fundamental questions about electron transport in amorphous organic metals and suggests exciting new applications for these materials.

6.2 Introduction

Conducting organic materials underpin technologies ranging from displays to flexible electronics.[1] This broad family includes doped organic polymers,[2] molecular conductors,[3,4] and conducting coordination polymers.[5] Realizing high electrical conductivity in traditionally

insulating organic materials necessitates tuning their electronic structure through chemical doping.[6] Nevertheless, loss of doping on air exposure degrades conductivity in these materials. Materials that are intrinsically conductive, such as single-component molecular conductors,[7,8] are more robust to electronic changes but require crystallinity for metallic behavior. However, commercial organic materials are frequently purposefully amorphous to enhance durability and processability.[9] Using molecular design to engender high conductivity in undoped amorphous materials would enable tunable and robust conductivity in many applications, but there are no intrinsically conducting organic materials which maintain high conductivity when completely disordered.[10] Inorganic glassy metals have been discovered but require careful fabrication.[11] Furthermore, the relationship between metallic behavior, which classically requires periodicity giving rise to a well-defined band structure,and geometric disorder in these materials is still unclear.[12]

Electron-rich and redox-active tetrathiafulvalene (TTF) motifs feature prominently as molecular building blocks in conducting materials.[8] Appending thiolate groups to TTF to generate tetrathiafulvalene-tetrathiolate (TTFtt) enables the formation of extended coordination polymers that combine the properties of TTF with the rich electronic structures of transition metal dithiolenes.[13] While the promise of these materials has been recognized, their structure, purity, composition, and hence properties are not well-defined due to synthetic challenges.[14] We recently discovered syntheses that enable the isolation of a series of redox congeners of capped TTFtt compounds and their facile transmetalation to group 10 metals.[15] Here we report that this synthetic strategy enables the isolation of the material NiTTFtt in high purity as an amorphous powder. Despite its disordered structure (Fig. 6.1, NiTTFtt exhibits remarkably high conductivity of 1280 S/cm (room temperature, four-probe measurement) and intrinsically glassy metallic behavior. Advanced theoretical analysis shows that these properties are enabled by strong molecular overlap and correlation that are robust to structural perturbations. This unusual set of structural and electronic

features results in remarkably stable conductivity which is maintained in air for weeks and at temperatures up to 140 °. The unusual properties of NiTTFtt demonstrate that molecular design can enable metallic conductivity even in completely disordered materials. This finding raises fundamental questions about charge transport mechanisms in disordered materials and suggests exciting new applications for intrinsically metallic organic materials.

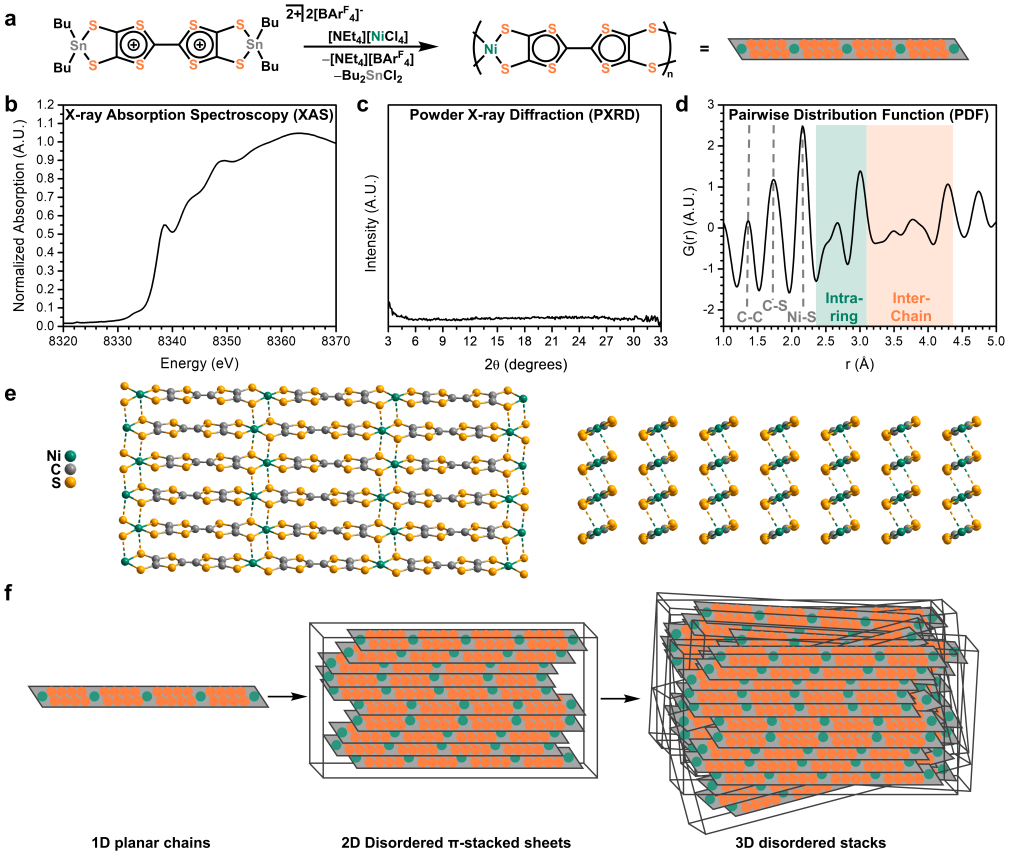

Figure 6.1: Synthesis and structure of NiTTFtt. a: Synthetic scheme. b: PXRD data.c: PDF data. d: XAS spectrum. e:Modeled structure. f:Hierarchical structure showing molecularly ordered chains but disordered packing in sheets and stacks.

6.3 Band Structures and Metallicity

One common form of analysis using band structures is to categorize the material as an insulator, semiconductor, semimetal, or metal. The metric used to categorize these materials

is the ability for electrons to transition between conduction and valence bands, since conductivity is directly related to electron flow in the conduction band. There are two main factors that control the degree to which this transition is able to occur: energetics and momentum.[16] If the band gap (the smallest energetic difference between the conduction and valence bands) is large, then the energy cost to transition to the conduction band is large and therefore the transition is unlikely. Additionally, these transitions can be accompanied by a change in electron momentum, which corresponds to changing the electron's position in the Brillouin Zone. In these cases, due to the conservation of momentum, the transition must be accompanied by a phonon mode and therefore is more likely in materials that are more susceptible to maintaining phonon modes. Generally, this property is dependent on the entire band structure and the momentum of the transition itself,[17] and therefore is significantly more difficult to characterize than the energetic factor. We will largely focus on the energetics here, and leave the phonon mode characterization for future work.

Insulators and semiconductors are defined by a Fermi level that doesn't cross any bands, with insulators typically being defined as having a band gap greater than 4 eV and semiconductors having a band gap of at most 4 eV. The band gap threshold separating semiconductors and insulators isn't uniquely defined from a theoretical perspective, but rather simply used as an approximate tool for categorizing the properties of these systems. Realistically, these materials are categorized by their physical properties which correspond roughly to this electronic structure definition related to the band gap.

By contrast, semimetals and metals have zero band gap, meaning that a band crosses the Fermi level. The distinction between semimetals and metals comes from the density of states,[18] with semimetals having a low density of states at or around the Fermi level and metals having a high density of states at or around the Fermi level. Like the distinction between insulators and semiconductors, the particular density of states that separates semimetals from metals isn't uniquely defined and is simply used as an approximate tool. Typically, a

low density of states for a semiconductor either comes from valence and conduction bands that meet at a single point at the Fermi level, or from bands that cross at several points in the band structure, leaving the Fermi level outside of any band between crossings.

6.4 NiTTFtt Electronic structure

Density functional theory calculations were undertaken on 1D chains and 3D stacks of NiTTFtt based on the structural model in Fig. 6.1. To approximate the disordered 3D structure, we chose unit cell geometries with one or two chains in the unit cell, which we'll call the 3D monomer and 3D dimer systems. A 1D monomer unit cell was then constructed by increasing the unit cell side lengths other than the chain axis, to approximate a vacuum in those directions. In this context, the terms monomer and dimer are used to distinguish between the number of subunits in a unit cell, but in all cases periodic boundary conditions are applied. By contrast, calculations without periodic boundary conditions will use the terms molecular and bimolecular to distinguish the number of NiTTFtt subunits in the calculation.

We determine the band structure and density of states for the 1D monomer, 3D monomer, and 3D dimer systems using Density Functional Theory (DFT) in Quantumespresso.[19,20] The kinetic energy cutoff of basis plane-wave functions (100 Ry), Marzari-Vanderbilt-DeVita-Payne cold smearing[21] temperature (0.001 Ry), energy convergence threshold (1e-8 Ry), and k-point sampling were optimized to reduce error in the band structure. All calculations used a PAW pseudopotential with a PBE functional and a nonlinear core correction from PSlibrary.[22,23] Brillouin zones are generated by the SeeK-path tool,[24,25] and only relevant points used in the band structure of the primitive cell were included for clarity.

The 2-subunit unit cell geometry predicted by PXRD was used for 3D dimeric model calculations, with k-point sampling using a 5×5×5 Monkhorst-pack grid. Additionally, the dimeric structure was reduced to a monomeric unit cell such that the neighboring chains have the same glide symmetry as the dimeric unit cell using a triclinic box. These 3D

monomeric calculations were then performed using a 9×3×6 Monkhorst-pack grid. Finally, the 3D monomeric unit cell was altered to have side lengths of 50 angstroms (leaving only the chain-axis box length unaltered) to create a quasi-1D unit cell. Calculations on this system were performed using a 9×1×1 Monkhorst-pack grid. The density of states plots for both 3D systems show significant density around the Fermi level, indicating that the 3D systems are metallic. By contrast, the 1D monomer shows very little density around the Fermi level. Combined with the crossing of bands at the Fermi level at the gamma-point, this indicates that the 1D monomer is semimetallic. The packing of chains into a 3D structure causes a transition from semimetal to a metal. Likewise, the band structures for both 3D systems have several bands crossing the Fermi level, further indicating that the 3D system is metallic.

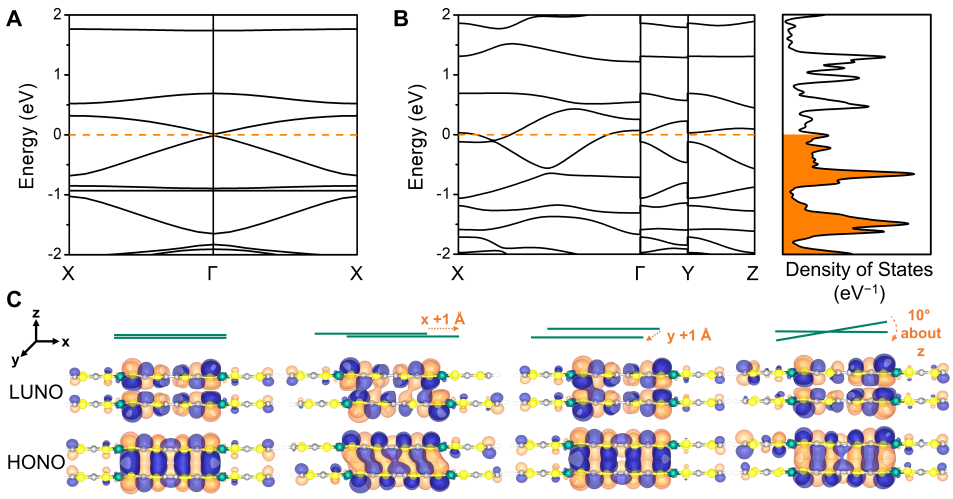

Figure 6.2: Theoretical analysis of NiTTFtt. a: Computed band structure of an isolated chain. b: Computed band structure of the idealized 3D structure determined from experimental data. c: Orbital diagrams of a molecular dimer of NiTTFtt building blocks showing that significant overlap is maintained regardless of structural distortions.

Interestingly, isolated 1D chains of NiTTFtt show semi-metallic behavior but exhibit a metallic band structure upon 3D assembly (Fig. 6.2a and b respectively). Analysis of the band structure shows that metallic character arises from both π-stacking interactions within the 2D sheets (Γ to Z), as well as side-to-side S–S interactions between sheets which broaden the bands near the Fermi level (Γ to X). Similar interactions have been invoked in

single-component molecular conductors.[7]

Additionally, a bimolecular model was constructed from the NiTTFtt solid structure to emulate the inter-layer interactions present in the amorphous extended structure, with the individual unit displayed in Fig. 6.2c. An inter-layer distance of 3.35Å was chosen based on the average distance in the proposed structure. The results for B3LYP[26]/6-31G*[27] with the GD3BJ[28] dispersion correction and [20,20] active space variational 2-electron reduced density matrix (v2RDM)[29–31]/6-31G[32] calculations are displayed in Table 6.1. To further understand the energetics of the inter-unit displacements, CASSCF calculations were carried out with the v2RDM method and a large active space of 20 electrons distributed in 20 molecular orbitals ([20,20]) with a 6-31G basis set.

Similar molecular systems containing $TTFtt^{2+}$units have previously been shown to exhibit multi-reference correlation in their electronic structure and as such DFT is not sufficient for their description.[15] Indeed, our calculations show that all model systems display multi-reference correlation, with the degree of biradical character exhibited depending on the alignment of the two units. Fig. 6.2c displays the highest occupied natural orbital (HONO) and lowest unoccupied natural orbital (LUNO) and their occupation numbers (NON) for each of the three studied spatial arrangements. The symmetrically aligned top structure exhibits the lowest degree of multi-reference character, however, with HONO and LUNO occupations of 1.55 and 0.41, it nonetheless displays a significant amount of strong correlation and biradical character. In this arrangement the HONO and LUNO split into one orbital that is clearly bonding across the π stack and shows good overlap across the two individual NiTTFtt units, the HONO, and one orbital that is anti-bonding across the π stack and shows no density bridging the two individual units, the LUNO.

	B3LYP/6-31G*			[20,20] v2RDM/6-31G						
	ΔE	ΔH	ΔE_{MO}	ΔE	ΔH	ΔE_c	λ_{385}	λ_{386}	λ_{387}	λ_{388}
top			32.88			-246.43	1.70	1.55	0.41	0.29
para	-6.3	-3.99	20.88	-33.43	-31.64	-291.03	1.56	1.19	0.84	0.42
perp	-4.8	-3.1	26.87	-25.5	-24.9	-259.33	1.60	1.34	0.63	0.20
angle	0.8	2.0	34.54	-10.7	-9.5	-255.60	1.68	1.55	0.44	0.33

Table 6.1: Electronic energy and enthalpy differences (in kcal/mol) of the parallel (para), perpendicular (perp) shifted and 10° twisted (angle) structures versus the symmetrically aligned (top) structure. ΔE_{MO} denotes the LUMO-HOMO gap in millihartree, E_c denotes the electronic correlation energy, defined as $E_{v2RDM} - E_{HF}$ in millihartree, and λ_N denotes the occupations of the Nth natural orbital.

6.5 Invariance with respect to geometry

A series of calculations were performed on a modified 3D monomeric unit cell, such that the lattice vectors align with the chain, pi-stacking, and plane-stacking axes. Slight variations in pi-stacking lattice vector were chosen such that neighboring chains are shifted along the chain axis relative to each other, to compare to the molecular calculations. Shift lengths of 0.5 angstroms, 1.0 angstroms, and 1.5 angstroms were chosen, each with k-point sampling using a 3×3×9 Monkhorst-pack grid.

In addition to these periodic calculations, we have also analyzed why the metallic character of NiTTFtt is maintained with disorder by examining molecular models which can be systematically distorted (Fig. 6.2). Two molecular fragments of NiTTFtt were fixed at positions which vary the slip, π-stacking, and side-to-side distances as well as the interchain twist angle. The electronic structures of these models were analyzed by variational 2-electron reduced density matrix (v2RDM) complete active space self-consistent field (CASSCF) calculations.[31] This analysis demonstrates that the molecular fragments of NiTTFtt have significant overlap and correlation that is remarkably robust to disorder. This is perhaps best illustrated by the fact that the HONO-LUNO gaps have little to no change with structural distortions(Table 6.1). These computations explain how metallic character is preserved in amorphous NiTTFtt: periodicity is disrupted by small scale structural disorder, but these

defects are not significant enough to disrupt overlap, correlation, and delocalization.

Both parallel as well as perpendicular displacements of the individual NiTTFtt units result in significant increases in multi-reference correlation. The *para* structure exhibits near-biradical NON of 1.19 and 0.81 for the HONO and LUNO, respectively, and additional significant fractionalization in the HONO-1 and LUNO+1, which display NON of 1.56 and 0.42 as compared to 1.70 and 0.29 in the top structure, while the *perp* arrangement shows slightly less significant but still noteworthy changes to the HONO and LUNO occupations with $\lambda_{HONO} = 1.31$ and $\lambda_{LUNO} = 0.63$. In both cases these changes in the NON are accompanied with corresponding changes to the natural orbitals and in both shift arrangements we observe inter-unit overlap in the LUNO along the π-stacking axis. Lastly, the introduction of a 10° twist angle shows no significant changes in the frontier natural orbital occupations and the natural orbital densities. The trends displayed by the NON mirror those of the LUMO-HOMO gaps calculated with DFT; ΔE_{MO} decreases as we shift the NiTTFtt units and fractionalization in the v2RDM HONO and LUNO increases.

6.6 Conclusions

Comparison of periodic and molecular calculations under various structural deformations reveals a relatively flat potential energy surface, which agrees with the experimental determination that the system can form an amorphous structure. Despite the disordered structure, the band structure of our periodic models indicates that the system is metallic for all structural deformations calculated, suggesting that any local configurations of chains in the amorphous structure will likely maintain metallicity. Although amorphous materials don't have a well-defined crystalline structure, the models we use approximate the structure of NiTTFtt by periodically repeating a local configuration across all of space. This approximation neglects long-range disordered interactions, which could be the subject of future work.

With 2 subunits are considered in a system, there are 6 structural parameters describing the relative orientation of the chains, and we studied 3 of them individually (two shift distances and one twist angle); PXRD calculations showed that the remaining 3 degrees of freedom were determined to be unimportant to describe the metallicity and structure of the amorphous material. For a calculation with N subunits in the unit cell, there are $6(N-1)$ independent structural parameters to be analyzed, which will need to be studied more extensively.

Finally, analysis using the molecular v2RDM theory shows significant fractional occupation and natural orbital overlap between molecular subunits. The correlation between subunits persists even after structural deformation, indicating that correlation likely exists at long range in the amorphous material, and as such any future theoretical treatment of this system should include static correlation. This result demonstrates the need to capture static correlation to recover a complete picture of the electronic structure of NiTTFtt.

Organic conductors are an enormously important class of materials. To realize conductivity in normally insulating organic materials it is typically necessary to optimize their electronic structure through doping and their geometric structure through crystallinity. However, the requirement for doping and crystallinity imposes restrictions on composition and stability. Here we report an unusual new material, NiTTFtt, that is structurally amorphous, precluding a classical band structure. Nevertheless, detailed characterization of NiTTFtt reveals high conductivity and metallic character. Theory shows that the presence of this metallic behavior is enabled by significant overlap between the molecular units of NiTTFtt that is insensitive to structural distortions. NiTTFtt shows that some interesting phenomena discussed in all-inorganic glassy metals are present in organic materials composed of significantly more complex and tunable molecular building blocks. Regardless, the juxtaposition of metallic character and disorder in NiTTFtt provides remarkable thermally and aerobically stable conductivity. These results demonstrate that the use of molecular units that

have strong overlap, and subsequently strong electronic delocalization, can lead to metallic character even in completely amorphous materials.

References

(1) Guo, X.; Facchetti, A. The journey of conducting polymers from discovery to application. *Nature materials* **2020**, *19*, 922–928.

(2) Heeger, A. J. Nobel Lecture: Semiconducting and metallic polymers: The fourth generation of polymeric materials*. *Reviews of Modern Physics* **2001**, *73*.

(3) Bryce, M. R. Recent progress on conducting organic charge-transfer salts. *Chemical Society Reviews* **1991**, *20*, 355–390.

(4) Valade, L.; de Caro, D.; Faulmann, C.; Jacob, K. TTF[Ni(dmit)2]2: From single-crystals to thin layers, nanowires, and nanoparticles. *Coordination Chemistry Reviews* **2016**, *308*, 433–444.

(5) Xie, L. S.; Skorupskii, G.; Dincă, M. Electrically Conductive Metal-Organic Frameworks. *Chemical Reviews* **2020**, *120*, 8536–8580.

(6) Bubnova, O. et al. Semi-metallic polymers. *Nature Materials* **2013**, *13*, 190–194.

(7) Kobayashi, A.; Fujiwara, E.; Kobayashi, H. Single-Component Molecular Metals with Extended-TTF Dithiolate Ligands. *Chemical Reviews* **2004**, *104*, 5243–5264.

(8) Kobayashi, Y.; Terauchi, T.; Sumi, S.; Matsushita, Y. Carrier generation and electronic properties of a single-component pure organic metal. *Nature materials* **2017**, *16*, 109–114.

(9) Venkateshvaran, D. et al. Approaching disorder-free transport in high-mobility conjugated polymers. *Nature* **2014**, *515*, 384–388.

(10) Joo, Y.; Agarkar, V.; Sung, S. H.; Savoie, B. M.; Boudouris, B. W. A nonconjugated radical polymer glass with high electrical conductivity. *Science* **2018**, *359*, 1391–1395.

(11) Plummer, J. Is metallic glass poised to come of age? *Nature Materials* **2015**, *14*, 553–555.

(12) Hirata, A.; Kang, L. J.; Fujita, T.; Klumov, B.; Matsue, K.; Kotani, M.; Yavari, A. R.; Chen, M. W. Geometric frustration of icosahedron in metallic glasses. *Science* **2013**, *341*, 376–379.

(13) Eisenberg, R.; Gray, H. B. Noninnocence in metal complexes: A dithiolene dawn. *Inorganic Chemistry* **2011**, *50*, 9741–9751.

(14) McCullough, R. D.; Belot, J. A.; Seth, J.; Rheingold, A. L.; Yap, G. P.; Cowan, D. O. Building block ligands for new molecular conductors: homobimetallic tetrathiafulvalene tetrathiolates and metal diselenolenes and ditellurolenes. *Journal of Materials Chemistry* **1995**, *5*, 1581–1587.

(15) Xie, J.; Boyn, J. N.; Filatov, A. S.; McNeece, A. J.; Mazziotti, D. A.; Anderson, J. S. Redox, transmetalation, and stacking properties of tetrathiafulvalene-2,3,6,7-tetrathiolate bridged tin, nickel, and palladium compounds. *Chemical Science* **2020**, *11*, 1066–1078.

(16) Harrison, W. A., *Electronic Structure and the Properties of Solids : the Physics of the Chemical Bond.* Dover Publications: 1980.

(17) Verstraete, M. J.; Gonze, X. Phonon band structure and electron-phonon interactions in metallic nanowires. *Physical Review B* **2006**, *74*, 153408.

(18) Beer, A., *Semiconductors and Semimetals*; Willardson, R. K., Ed.; Academic Press: 1966; Vol. 1.

(19) Giannozzi, P. et al. QUANTUM ESPRESSO: A modular and open-source software project for quantum simulations of materials. *Journal of Physics Condensed Matter* **2009**, *21*, 395502.

(20) Giannozzi, P. et al. Advanced capabilities for materials modelling with Quantum ESPRESSO. *Journal of Physics: Condensed Matter* **2017**, *29*, 465901.

(21) Marzari, N.; Vanderbilt, D.; Vita, A. D.; Payne, M. C. Thermal Contraction and Disordering of the Al(110) Surface. *Physical Review Letters* **1999**, *82*, 3296.

(22) Prandini, G.; Marrazzo, A.; Castelli, I. E.; Mounet, N.; Marzari, N. Precision and efficiency in solid-state pseudopotential calculations. *Computational Materials* **2018**, *4*, DOI: 10.1038/s41524-018-0127-2.

(23) Lejaeghere, K. et al. Reproducibility in density functional theory calculations of solids. *Science* **2016**, *351*, DOI: 10.1126/science.aad3000.

(24) Hinuma, Y.; Pizzi, G.; Kumagai, Y.; Oba, F.; Tanaka, I. Band structure diagram paths based on crystallography. *Computational Materials Science* **2017**, *128*, 140–184.

(25) Togo, A.; Tanaka, I. Spglib: a software library for crystal symmetry search. *Arxiv* **2018**, DOI: 10.48550/arxiv.1808.01590.

(26) Becke, A. D. Density-functional thermochemistry. III. The role of exact exchange. *The Journal of Chemical Physics* **1998**, *98*, 5648.

(27) Francl, M. M.; Pietro, W. J.; Hehre, W. J.; Binkley, J. S.; Gordon, M. S.; DeFrees, D. J.; Pople, J. A. Self-consistent molecular orbital methods. XXIII. A polarization-type basis set for second-row elements. *The Journal of Chemical Physics* **1982**, *77*, 3654.

(28) Grimme, S.; Ehrlich, S.; Goerigk, L. Effect of the damping function in dispersion corrected density functional theory. *Journal of Computational Chemistry* **2011**, *32*, 1456–1465.

(29) Gidofalvi, G.; Mazziotti, D. A. Active-space two-electron reduced-density-matrix method: Complete active-space calculations without diagonalization of the N -electron Hamiltonian. *Journal of Chemical Physics* **2008**, *129*, 134108.

(30) Mazziotti, D. A. Variational minimization of atomic and molecular ground-state energies via the two-particle reduced density matrix. *Phys. Rev. A* **2002**, *65*, 62511.

(31) Mazziotti, D. A. Large-scale semidefinite programming for many-electron quantum mechanics. *Physical Review Letters* **2011**, *106*, 083001.

(32) Hehre, W. J.; Ditchfield, K.; Pople, J. A. Self-Consistent Molecular Orbital Methods. XII. Further Extensions of Gaussian—Type Basis Sets for Use in Molecular Orbital Studies of Organic Molecules. *The Journal of Chemical Physics* **1972**, *56*, 2257.